



# WPI

## Articulating Wind Turbine

A Major Qualifying Project to be submitted to the Faculty of Worcester Polytechnic Institute  
in partial fulfillment of the requirements for the degree of Bachelor of Science

Submitted by:

Morgan Boyd  
Matthew Jackson  
Anne Cecilie Jacobsen  
Jason Lackie  
Patrick Rosica

Submitted to:

Project Advisors:

Brian Savilonis, Worcester Polytechnic Institute

April 30, 2015

*This report represents work of WPI undergraduate students submitted to the faculty as evidence of a degree requirement. WPI routinely publishes these reports on its web site without editorial or peer review. For more information about the projects program at WPI, see <http://www.wpi.edu/Academics/Projects>.*

## Abstract

There is a growing market for Wind Energy, where Vertical Axis Wind Turbines (VAWT) are currently overshadowed by Horizontal Axis Wind Turbines (HAWT). While the efficiencies of VAWTs are currently lower than that of their horizontal counterparts, there are significant areas for growth in the VAWT market due to the wide variety of applications. The goal of this project is to investigate improvements on VAWTs by designing and developing articulating blades such as those found in Schneider Propellers. The prototype was designed with airfoils with the capability of both articulating and being fixed. In testing it was found that the fixed airfoil design did not start operating at the available wind speeds. At these same wind speeds, it was found that the articulating airfoil design had a maximum efficiency of approximately 10% and produced 7.4 W.

## Acknowledgements

The team would like to thank Professor Brian Savilonis for his guidance in the completion of this project. Frederick Hutson for lending us the Vernier Force Gauge for testing as well as Professor Sergey Makarov for lending us his hot wire cutter for the manufacturing of the airfoils. We would also like to thank Barbara Furhman for her help in all purchasing for the project. Lastly we would like to thank the Massachusetts Police at the Worcester Regional Airport for letting us complete the testing at the airport.

## Table of Contents

Abstract .....	2
Acknowledgements .....	3
Table of Figures .....	iv
List of Tables .....	vii
List of Equations .....	viii
Chapter 1: Introduction .....	1
Chapter 2: Background .....	2
2.1 Wind Power .....	2
2.2 Airfoils .....	2
2.2.1 Lift.....	3
2.2.2 Drag.....	4
2.2.3 NACA Airfoils.....	4
2.3 Wind Turbine Types .....	5
2.4 Schneider Propeller.....	8
Chapter 3: Design Process .....	11
3.1 Design Specifications.....	11
3.2 Design Selection .....	12
3.3 Airfoil Selection.....	12
3.4 Articulating Airfoil Design .....	14

3.5 Initial Calculations .....	16
Chapter 4: Predictive Calculations.....	21
Chapter 5: Construction .....	25
5.1 Base.....	25
5.2 Prony Brake .....	27
5.3 Airfoil plates .....	30
5.4 Ball bearings .....	31
5.5 Airfoil plate attached to the base .....	31
5.6 Airfoil Construction.....	32
5.7 Spring Attachment System .....	35
Chapter 6: Testing.....	38
6.1 Phase I: Proof of Concept .....	38
6.2 Phase II: RPM Testing .....	38
6.3 Phase III: Torque.....	39
Chapter 7: Results .....	40
7.1 Phase I: Proof of Concept .....	40
7.1.1 Starting Torque .....	40
7.2 Phase II: RPM Testing .....	41
7.3 Phase III: Torque Testing.....	44
Chapter 8: Analysis.....	48

8.1 Power .....	48
8.2 Efficiency .....	49
Chapter 9: Conclusions .....	52
Chapter 10: Recommendations .....	53
10.1 Friction .....	53
10.2 Manufacturing .....	53
10.3 Testing .....	54
References .....	55
Appendix A: Predicted Lift and Drag Algebra .....	57
Appendix B: Detailed Predictive Calculations .....	59
Appendix C: Computer Aided Design Drawings .....	60
Appendix D: Turbine Starting Time Calculations .....	64
Appendix E: Torque Testing Results .....	66

## Table of Figures

Figure 1: Wind Turbine .....	2
Figure 2: Anatomy of an Airfoil .....	3
Figure 3: Airfoil Schematic .....	3
Figure 4: Horizontal axis wind turbine .....	5
Figure 5: Darrieus Turbine.....	6
Figure 6: Power coefficient and tip speed ratio of different turbines .....	8
Figure 7: Schneider Propeller on Ferry.....	9
Figure 8: Blade Steering Curve Example (Jurgens) .....	9
Figure 9: Directional Thrust Diagrams (Yamada) .....	10
Figure 10: NACA 2412 Coefficient of Lift versus Alpha .....	13
Figure 11: NACA 2412 Coefficient of Drag versus Alpha .....	13
Figure 12: Profile Used to Cut Airfoils.....	14
Figure 13: Articulating airfoil design using bungee cords.....	15
Figure 14: CAD Model of design .....	16
Figure 15: Mean Wind Speeds Over a Year .....	17
Figure 16: Forces and Velocities Acting on a Vertical Axis Wind Turbine.....	22
Figure 17: Calculated Power vs Wind Speed graph .....	24
Figure 18: Screw placement for table leg .....	26
Figure 19: Supporting frame of table.....	26
Figure 20: Leg attachment .....	27
Figure 21: Prony Brake .....	28
Figure 22: Example prony brake.....	28

Figure 23: 90 degree angle motion adjustment.....	29
Figure 24: Constructed prony brake .....	29
Figure 25: Loose prony brake head .....	30
Figure 26: Tightened prony brake head .....	30
Figure 27: Airfoil plate .....	31
Figure 28: Ball Bearing.....	31
Figure 29: Shaft attachment collar .....	32
Figure 30: Cutting technique with the Manix Hot Wire Cutter .....	33
Figure 31: Plywood and screw supports used to align the foam.....	33
Figure 32: Placement of the 5/8” holes on Airfoil.....	34
Figure 33: Wooden profile and the location of nails .....	34
Figure 34: Complete airfoil.....	35
Figure 35: Eyehook attachment .....	36
Figure 36: Spring Attachment Piece .....	36
Figure 37: Final spring configuration .....	37
Figure 38: Vernier Force Gauge Testing Set Up .....	39
Figure 39: RPM to Wind Speed.....	43
Figure 40: Torque Testing .....	44
Figure 41: Torque vs Wind Speed .....	45
Figure 42: Torque vs RPM .....	46
Figure 43: Derived Torque vs RPM.....	47
Figure 44: Calculated Power vs Wind Speed .....	49
Figure 45: Turbine Efficiency.....	50

Figure 46: Airfoil Design.....	60
Figure 47: Attachment Piece Design .....	61
Figure 48: Acrylic Base Plate Design.....	62
Figure 49: Shaft Design .....	63
Figure 50: SolidWorks Inertia .....	65
Figure 51: Torque Testing Graph 1 .....	66
Figure 52: Torque Testing Graph 2 .....	67
Figure 53: Torque Testing Graph 3 .....	68
Figure 54: Torque Testing Graph 4 .....	69

## List of Tables

Table 1: Comparison of HAWT and VAWT.....	7
Table 2: Hypothetical Turbine Calculations.....	19
Table 3: Predictive Power Calculation Variables for Fixed Turbine.....	23
Table 4: Predicted Power at Different Wind Speeds.....	24
Table 5: Phase I Table.....	40
Table 6: Phase II RPM wind speed Table (1).....	42
Table 7: Phase II RPM wind speed Table (2).....	42
Table 8: Lever Arm Calculation.....	44
Table 9: Wind Speed, RPM and Torque.....	46
Table 10: Power to Wind Speed.....	48
Table 11: Torque Testing Analysis 1.....	66
Table 12: Torque Testing Analysis 2.....	67
Table 13: Torque Testing Analysis 3.....	68
Table 14: Torque Testing Analysis 4.....	69

## List of Equations

Equation 1: Lift Force.....	4
Equation 2: Drag Force.....	4
Equation 3: Velocity Conversion.....	17
Equation 4: Rotational Speed.....	17
Equation 5: Ideal Power Produced.....	18
Equation 6: Torque Produced .....	18
Equation 7: Tip Speed Ratio.....	21
Equation 8: Resulting Velocity.....	22
Equation 9: Angle of Attack .....	22
Equation 10: Resultant equation.....	22
Equation 11: Power Equation .....	23
Equation 12: Torque, Inertia, and Angular Acceleration.....	41
Equation 13: Rotation, time and acceleration.....	41
Equation 14: Angular Velocity Calculation.....	41
Equation 15: Angular Velocity .....	43
Equation 16: RPM Correlation .....	43
Equation 17: Prony Break Torque Calculation.....	45
Equation 18: Torque Wind Speed Relation .....	45
Equation 19: Derived Torque vs RPM.....	46
Equation 20: Power Coefficient.....	50
Equation 21: Resultant equation .....	57
Equation 22: Lift force in X-Direction-Positive angle of attack.....	57

Equation 23: Lift Force in Y-Direction-Positive angle of attack.....	57
Equation 24: Drag Force in X-Direction-Positive angle of attack.....	57
Equation 25: Drag Force in Y-Direction-Positive angle of attack.....	57
Equation 26: Resultant Force-Positive angle of attack.....	57
Equation 27: Lift Force X-Direction-Negative angle of attack .....	57
Equation 28: Lift Force Y-Direction-Negative angle of attack .....	57
Equation 29: Drag Force X-Direction-Negative angle of attack .....	57
Equation 30: Drag Force Y-Direction-Negative angle of attack .....	58
Equation 31: Resultant Force Equation 1-Negative angle of attack.....	58
Equation 32: Resultant Force Equation 2-Negative angle of attack.....	58
Equation 33: Sum of Torques in operation.....	64
Equation 34: Evaluated sum of torques .....	64
Equation 35: Angular acceleration.....	64
Equation 36: Evaluated angular acceleration.....	64
Equation 37: Angular velocity with regards to time.....	64
Equation 38: Angular velocity integral.....	64
Equation 39: Angular position with regards to time.....	64
Equation 40: Evaluated angular position with regards to time.....	64

## Chapter 1: Introduction

The combustion of fossil fuels for energy has a negative effect on the globe as the emission of carbon dioxide and other greenhouse gasses contribute to the effects of global warming (United States Environmental Protection Agency , 2015). To maintain the growth of civilization today, the need for energy is ever increasing and if the dependency on fossil fuels to provide this energy continues, the effects of global warming could be catastrophic (NASA, 2015). One way to prevent this outcome is to decrease the dependency on fossil fuels and move towards more renewable sources of energy. One such growing source of energy is wind power (International Energy Agency, 2015).

Wind turbines are categorized by their axis of rotation; Horizontal Axis Wind Turbines (HAWT) and Vertical Axis Wind Turbines (VAWT). The most common wind turbine is the HAWT, due to its superior efficiency (Muhammad Mahmood Aslam Bhutta, Renewable and Sustainable Energy Reviews, 2011). Since the goal of producing wind turbines is to harness as much of the available power in the wind as possible, the more efficient turbines have seen significantly higher use across the world. HAWTs are more costly to produce than VAWT's due to expensive materials and relatively complicated designs (Sandra Eriksson, 2008).

Even though the overall efficiency of HAWTs is higher than VAWTs, there are still several advantages of VAWT. For example, VAWTs have the possibility of functioning in areas where the horizontal turbines cannot. This is due to the functionality of the blades and the axis of rotation being independent of wind direction; therefore they can function in areas of turbulent wind flow (Muhammad Mahmood Aslam Bhutta, Renewable and Sustainable Energy Reviews, 2011). Due to VAWT's blade geometry, they are also less restricted by their potential surroundings and are not limited to laminar flow.

Due to some of these advantages of the vertical axis turbines, the team came with the goal of exploring ways to potentially improve upon the efficiency of VAWTs. If VAWTs were more efficient, there might be a potential market for them to be produced for a variety of applications. The more specific goal for the project was to build and test a vertical axis wind turbine with the intention to test potential improvements to the turbine's performance. The team constructed a Schneider Propeller inspired wind turbine that has both articulating and non-articulating airfoils to test the difference in performance between the two. The conclusions drawn in this study shows the potentially improved VAWT performance by using articulating airfoils.

## Chapter 2: Background

At the beginning of the project, the team conducted a literature review of the material necessary to complete this project. The material investigated included the core ideas and mathematical concepts for each section. The main topics covered incorporated into this review are airfoils, wind turbine types and Schneider Propellers.

### 2.1 Wind Power

Wind power is the transformation of wind energy into a more useable form such as electrical or mechanical. The earliest known example of wind power being utilized to operate a machine is the wind-powered organ created by Heron of Alexandria, a Greek engineer from the first century. Heron's design featured a wind wheel that could be turned into the wind for maximum power, as seen in Figure 1 below (Shuttleworth, 2014).

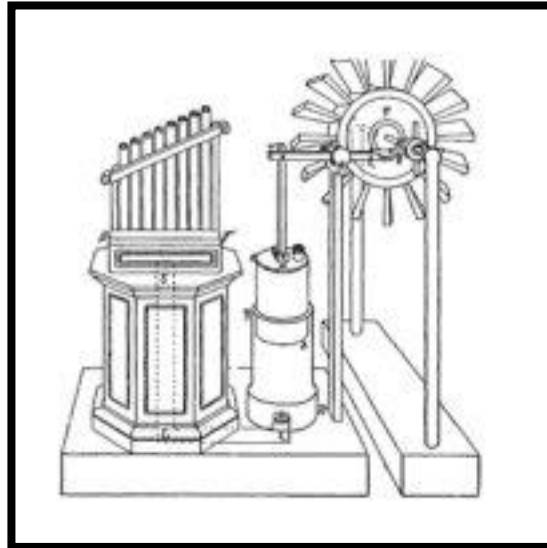


*Figure 1: Wind Turbine*

Wind Power technology has seen many innovations since Heron's work and continues to evolve to this day. There are many different windmills that have their own individual advantages due to facts such as their cost, manufacturability, and efficiency. New models continued to be theorized and tested in hopes of finding a better way to harness wind energy.

### 2.2 Airfoils

Airfoils are also utilized in wind turbines in order to generate higher torques and greater rotational velocities. An airfoil is a specialized structure with curved surfaces designed to give an optimal ratio of lift to drag for the purpose of flight, as applied to an aircraft. The parts of an airfoil are illustrated and described below in Figure 2.

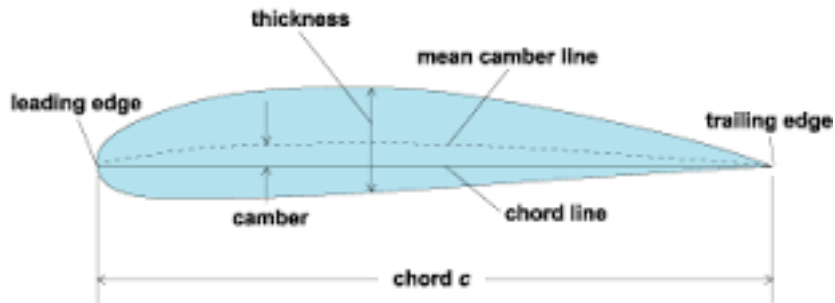


Figure 2: Anatomy of an Airfoil

- The *leading edge* is the point at the front of the airfoil with maximum curvature.
- The *trailing edge* is the point of maximum curvature at the rear of the airfoil.
- The *chord line* is the straight line connecting the leading and trailing edge.
- The *chord* is the length of the chord line.
- The *mean camber line* is the line of points equidistant between the upper and lower surfaces.
- The *thickness* is the distance between the upper and lower surfaces.
- The *camber* is the asymmetry between the top and bottom of the airfoil.

### 2.2.1 Lift

Lift is caused when the wind is split by the leading edge of the airfoil. The curved upper surface causes the air to accelerate and creates a pocket of low-pressure air as demonstrated in Figure 3. Air always moves towards lower pressure regions, so the relatively higher-pressure region under the wing pushes the wing up towards the lower pressure region. This phenomenon causes lift.

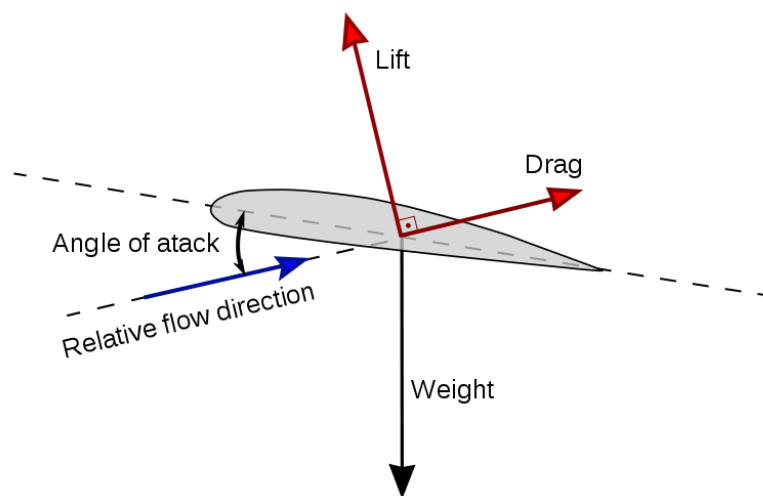


Figure 3: Airfoil Schematic

Lift can be found using Equation 1:

$$F_L = \frac{1}{2} \rho v^2 s C_l$$

*Equation 1: Lift Force*

Where:

- $F_L$  is the lift force.
- $\rho$  is the air density, which varies with altitude
- $v$  is the velocity of the air foil
- $s$  is the area of the airfoil
- $C_l$  is the lift coefficient, which is determined by the type of airfoil and the angle of attack and chord length. The angle of attack is the angle between the chord line and the velocity vector of the air.

### 2.2.2 Drag

Drag is a force acting in the opposite direction of relative motion of the airfoil. Drag has two primary components: parasitic drag and lift-induced drag. Parasitic drag is the drag caused by the interaction between the surface of the airfoil and the fluid it moves through. Lift induced drag is the drag that is created due to lift acting on the airfoil.

Drag can be found using Equation 2

$$F_D = \frac{1}{2} \rho v^2 A C_D$$

*Equation 2: Drag Force*

- $F_D$  is the drag force.
- $\rho$  is the air density, which varies with altitude
- $v$  is the velocity of the air foil
- $A$  is the cross sectional area of the airfoil
- $C_D$  is the drag coefficient, which is determined by the shape of the object and the Reynolds number. The Reynolds is the velocity times the characteristic diameter divided by the kinematic viscosity.

### 2.2.3 NACA Airfoils

The National Advisory Committee for Aeronautics (NACA) categorizes all airfoil shapes. In the four-digit airfoil series the first digit is the maximum camber as a percentage of the chord. The second digit is the location of the maximum camber in tens

of percent of the chord length from the leading edge. The last two digits describe the maximum thickness as a percentage of the chord. The lift coefficient and drag coefficient are values found through testing and have been tabulated for most of the four digit airfoils as classified by NACA.

A benefit of the NACA classification system is that coefficient of lift and coefficient of drag information has already been tabulated. Those values are experimentally based and using a NACA airfoil means that that information has been tabulated and does not need to be experimentally found.

### 2.3 Wind Turbine Types

There are two main types of wind turbines, Horizontal Axis Wind Turbines (HAWT) and Vertical Axis Wind Turbines (VAWT). All turbines belong to one of these two categories depending on which axis the blades rotate about. HAWTs rotate about the horizontal axis, as seen in Figure 4 below. This type of turbine is the most commonly produced commercial wind turbine.



*Figure 4: Horizontal axis wind turbine*

VAWTs rotate about the vertical axis, as seen in Figure 5 below. VAWTs are a less common turbine design and are not as widely commercially available.



*Figure 5: Darrieus Turbine*

Table 1 below shows a comparison of HAWT's and VAWTs, including some of the key aspects of each category of turbine, such as the sway seen in the tower as well as the overall area and impact on the surroundings.

	Vertical axis wind turbine (VAWT)	Horizontal axis wind turbine (HAWT)
Tower sway	Small	Large
Yaw mechanism	No	Yes
Self-starting	Yes	No
Overall formation	Simple	Complex
Generator location	On ground	Not on ground
Height from ground	Small	Large
Blade's operation space	Small	Large
Noise produced	Less	Relatively high
Wind direction	Independent	Dependent
Obstruction for birds	Less	High
Ideal efficiency	23%	59.3%

*Table 1: Comparison of HAWT and VAWT*

(Muhammad Mahmood Aslam Bhutta, Renewable and Sustainable Energy Reviews, 2011)

HAWTs are commercially popular because of the potential for 59.3% efficiency, which is the highest of in both classes of turbines (Muhammad Mahmood Aslam Bhutta, Renewable and Sustainable Energy Reviews, 2011). Unfortunately, HAWTs are not omnidirectional, and require a mechanism to rotate the head of the turbine so it faces the wind direction (Sandra Eriksson, 2008). This yaw mechanism adds complications to the manufacturing and maintenance of the turbine. Additionally the blades of HAWTs are complicated to design and manufacture. The single connection point to the shaft of the turbine creates additional stresses in the blades that must be accounted for in design and material choices (Sandra Eriksson, 2008).

VAWTs have a peak efficiency of 23%. Even though they are not as efficient as HAWTs, VAWTs do have several advantages. One of these advantages is that they are able to work in locations where the HAWT's do not yield a profitable efficiency, such as mountainous areas with turbulent air flow (Muhammad Mahmood Aslam Bhutta, Renewable and Sustainable Energy Reviews, 2011). Another positive aspect of the VAWT turbines is that they function with wind coming from any direction without any assistance from the user or a motor. A third positive aspect is that the stresses seen in the HAWT blades are not seen in VAWTs since they do not extend far from the shaft without support.

There are many different types of VAWTs, however the two that are most common are the Darrieus and the Savonius turbine. The Darrieus has a higher efficiency than many other VAWTs while the Savonius is favored because it has other features such as the ability to "self-start". This feature is necessary for purposes such as smaller scale home-use applications.

The ideal efficiency of the VAWTs is lower than the HAWTs. This large discrepancy can be attributed to the large amount of research that has been done on horizontal axis wind turbines compared to the less amount of research that been done on vertical axis wind turbines (Sandra Eriksson, 2008). Therefore the horizontal turbines have a lot more data supporting the ideal efficiency, as calculated by the Betz limit. The Betz limit is the maximum power that a turbine is capable of producing. Figure 6 below is a chart of the power coefficients and tip speed ratios of different types of turbines, showing the ideal efficiency as determined by Betz's law.

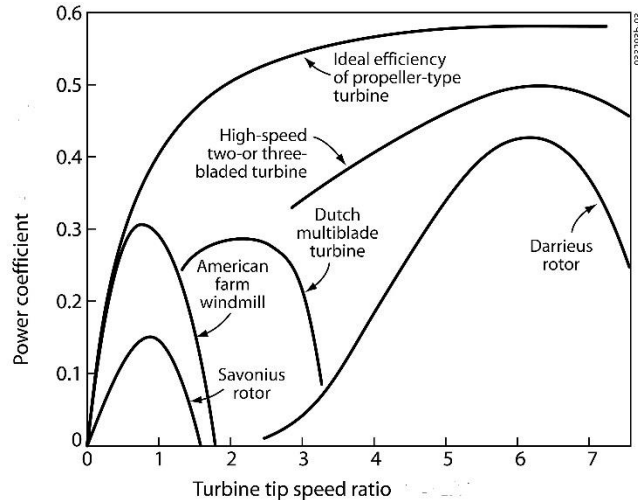


Figure 6: Power coefficient and tip speed ratio of different turbines

## 2.4 Schneider Propeller

Turbines and propellers work similarly with the main difference being the medium of operation. Due to the similar functionality the same aerodynamic properties apply to both devices. Therefore the team looked into the Schenider Propeller for design inspiration.

In 1927 Ernst Leo Schneider, a German mechanical engineer, created a new ship propeller called the Schneider Propeller. The propeller was designed to produce thrust in any direction, allowing ships to steer without having to change their heading.

Schneider propeller designs consist of a large circular rotating base or set of arms consisting of 3-6 hydrofoils. Each hydrofoil is fixed about an axis off the base and is controlled using two servo motors and a kinematic transmission. As the base rotates, each hydrofoil is orientated to provide thrust as needed. An example of the design is shown below in Figure 7.

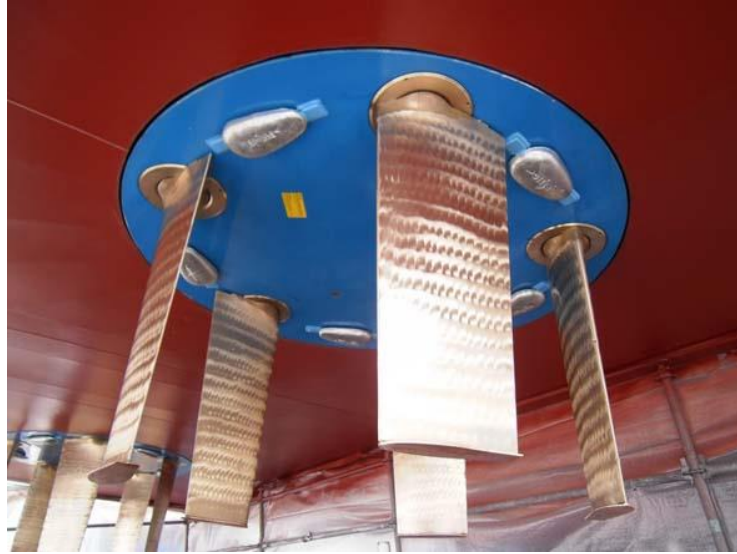


Figure 7: Schneider Propeller on Ferry

Schneider propellers' utilization of controlled articulating hydrofoils to create thrust is what sets them apart from other multidirectional propellers. In order to create the desired thrust, two different parameters must be met, steering angle ( $\alpha$ ) and phase angle ( $\phi$ ). This is done using the ship's power controls system which is operated by a member of the crew. The ship operator rotates the hydrofoils to generate thrust in a direction. This individually changes the steering angle on each hydrofoil to generate the desired thrust. This steering of the blades is accompanied with a certain phase angle. These two parameters can be graphed to create a blade steering curve (BSC). The BSC is a method to evaluate the amplitude and direction of thrust generated by the propeller. An example of a BSC is shown below in Figure 8 (Jurgens).

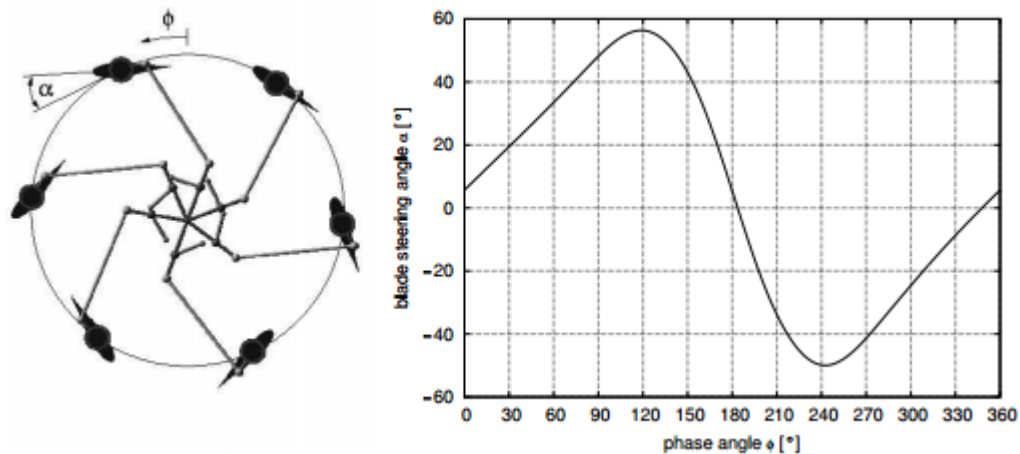


Figure 8: Blade Steering Curve Example (Jurgens)

With these two parameters satisfied, the operator is able to generate variable amounts of thrust in any direction. An example of the effects of steering angle is shown below in Figure 9.

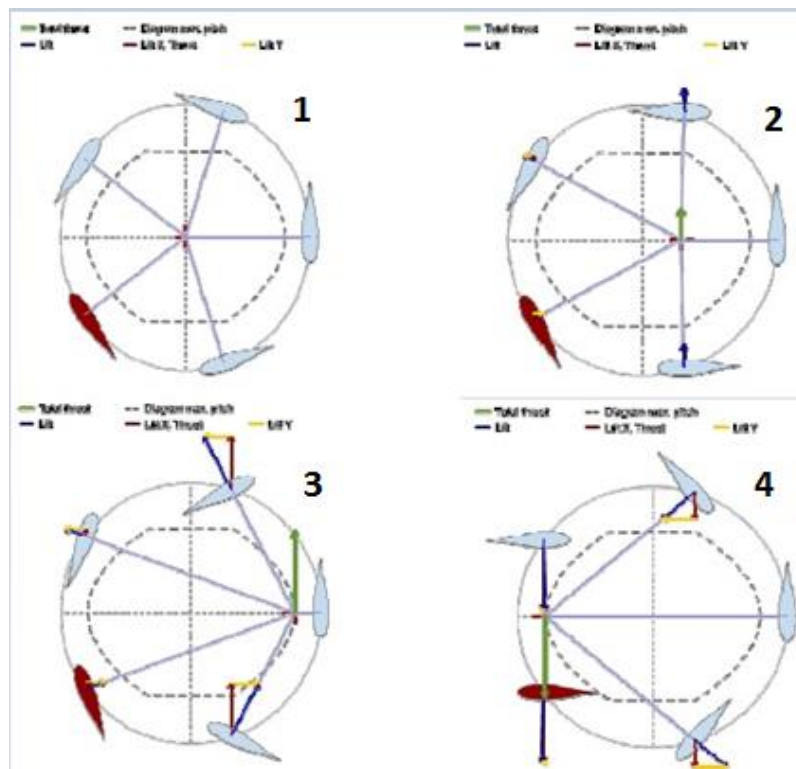


Figure 9: Directional Thrust Diagrams (Yamada)

The image above shows four different thrust demands on the Schneider propeller and the same phase angle. The first image, image 1, shows the propeller with no thrust demand. In this instance, the steering angle on each blade is zero resulting in the blades being tangential to the turbine. The second image shows the propeller with a 39% thrust demand ahead. This means that the operator is requesting 39% of the propellers full engine power to propel the boat ahead. In this image, notice the change in steering angle of the top most and bottom most blades. With this change in steering angle, the blades are producing a thrust vector shown in blue. These vectors sum to the green resulting vector shown in green. Using the propeller's ability to modify the steering angle of the blades, the turbine is able to produce directional specific thrust on command. This ability is the key reason Schneider propellers are effective propellers found in the tugboat industry as well as on many specialty vessels (Yamada).

## Chapter 3: Design Process

Once the appropriate background research had been done the team decided upon a final turbine design using the engineering design process. The original design intent was to investigate possible improvements on VAWTS to enhance their performance. Many different types and iterations of VAWTs were considered such as Darrieus and Savonius. From this investigation, the team concluded that there could be opportunity for improvement by modifying the pitch angle of the VAWT through articulating airfoils. To achieve this goal, the group drew inspirations and concepts from the Schneider propeller. The team used the Schneider propeller as a basic concept because the blades of a Schneider propeller articulate when spinning.

### 3.1 Design Specifications

The team developed a list of design specifications for the prototype in order to focus the design process. These design specifications were grouped by item and are listed below.

- Base
  - Lateral dimensions must not exceed 0.812 m (32 inches)
  - Must support at least 222 N (50 pounds) on center
  - Must include a center hole for shaft to pass through without interference
- Airfoils
  - Must provide appropriate lift to spin a VAWT of 0.457 m (18 inches) in diameter and maximum 89 N (20 pounds) in weight
  - Must include attachment holes on the top and bottom of airfoil to attach to the support plates
- Shaft
  - Must support and transfer the Vertical Axis rotation of the turbine
  - Must translate the vertical axis motion to horizontal axis motion for data collection
- Articulation System
  - Must allow for articulation of airfoil
  - Must prohibit the airfoils from striking any other components of the prototype
- Support plates
  - Must be able to support at most 89 N on center
  - Must include attachment points for the shaft and the airfoils
  - Must be made of a clear and see through material
- Measurement systems
  - Must be able to measure the force and torque of startup and steady state motion.
  - Must be able to measure the rotational speed of the device

- Must be able to measure the wind velocity at the time of testing
- Overall Functionality
  - Must be able start to spin with the force of the wind with no external force
  - Must be able to start to spin with both the airfoils fixed and the airfoils articulating
- Budget
  - Must have an overall cost of less than \$750 dollars

### 3.2 Design Selection

After the design specifications were decided upon, the initial design was created and the design and manufacturing of the prototype began. The design would consist of three airfoils, with the ability to both articulate and stay fixed, one shaft, two support plates and other connecting materials such as ball bearings, attachment collars and bolts.

The three airfoils would be placed at equal angles (120 degrees apart) to ensure a distributed and stable turbine. The airfoils were placed around the shaft of the turbine as close to the perimeter of the support plates as possible. By placing the airfoils as far away from the shaft as possible, the highest potential power output was found.

The two support plates, one for the top and the other for the bottom of the turbine, were made out of acrylic. The acrylic plates were chosen since they are clear and therefore would allow good visibility of the turbine while it was operating. The acrylic plates also provided adequate stability for the turbine without adding excessive weight.

The center shaft would be constrained to the support plates and to the base via a set of roller bearings. The shaft used was made of steel, originally the team had chosen an aluminum shaft since it has the desired stability and is significantly lighter than the steel counterpart. However, due to the size of the aluminum shaft and the size of the connection pieces, the aluminum shaft could not be used. The connection pieces were slightly smaller in diameter than the Aluminum shaft, so the pieces could not fit over the shaft. Therefore, the steel shaft was chosen for the final design. A computer aided design model (CAD) was created of the initial design in SolidWorks. The assembly of the design is shown below in Figure 14.

### 3.3 Airfoil Selection

For this project the team selected the NACA 2412, a non-symmetric airfoil. The non-symmetric airfoil was selected because the zero lift angle of attack ( $\alpha$ ) is less than zero degrees, allowing for more lift to be generated as it makes a full rotation. Below in Figure 10 and Figure 11 are the lift and drag coefficients versus  $\alpha$  graphs for the NACA 2412 airfoil. These graphs allow the designer to predict the lift and drag forces before testing the device.

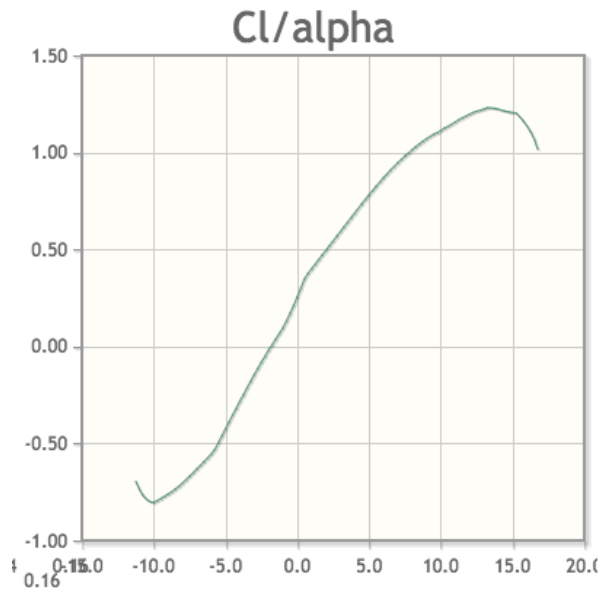


Figure 10: NACA 2412 Coefficient of Lift versus Alpha

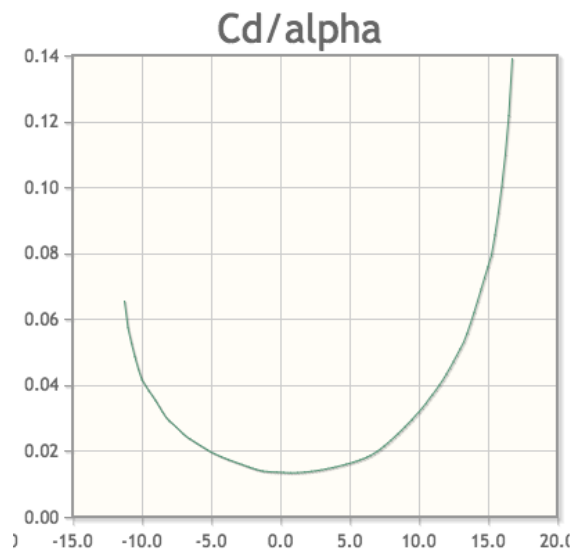


Figure 11: NACA 2412 Coefficient of Drag versus Alpha

An additional benefit of selecting the NACA 2412 airfoil is that it is one of the most common airfoils and would therefore be easy to purchase. If purchasing the airfoils were not an option, manufacturing would also be easier compared to other similar airfoils. One of the common problems with the manufacturing of airfoils is breaking the relatively thin trailing edge. With the NACA 2412 airfoils this is less likely due to their comparatively thicker trailing edge. The NACA 2412 profile is shown in Figure 12 below.



*Figure 12: Profile Used to Cut Airfoils*

### 3.4 Articulating Airfoil Design

The team made three iterations of the articulating system for the airfoils. The three iterations were designed so that all three could be tested once the turbine had been built and then the best design would be chosen for data collection.

The initial design of the articulation included a string pulley system. This system used a series of eyehooks and strings to attach the trailing edges of the airfoils to each other. Eyehooks would be attached to the bottom of each airfoils at the trailing edge. The string was then attached to the eyehook, wrapped around the shaft and then connected to the next airfoil. This system would fix the airfoils to each other so that if one airfoil traveled outwards (away from the shaft) it would pull the other two airfoils in towards the shaft in a continuous motion. For this design the team tried to optimize lift and drag since as one airfoil moved away from the shaft, it experienced lift forcing the other two airfoils to experience drag as they were pulled in towards the shaft.

The second design entailed the use of bungee cords, this design is shown in Figure 13 below. These bungee cords were constrained at the bottom of the airfoil and the center of the turbine, similarly to the previous string design. The bungee cords allowed for slightly more independent motion between the airfoils due to their “springy” nature.



*Figure 13: Articulating airfoil design using bungee cords*

The third and final design consisted of the use of springs. In this design the airfoils were not attached to each other and so their motion would not constrict each other. The springs would again be attached to the eyehooks at the base of the airfoils and the other end of the springs would be attached to an eyehook placed approximately two inches out from the base plate circumference. A detailed description of this design, with figures is shown in Chapter 5.

Based on initial testing of the turbine it was found that the airfoils were striking the center shaft of the turbine. Since the first two design iterations for the articulating motion did not prevent this motion the third design was chosen for data collection. Since the springs were attached to the outer perimeter of the turbine as opposed to the shaft, the inwards motion of the airfoils were controlled by the stiffness of the springs.

The SolidWorks drawing of the final design of the turbine, with the spring system in place is shown in Figure 14 below. The specific sizing of the turbine is justified through calculations in the following section.

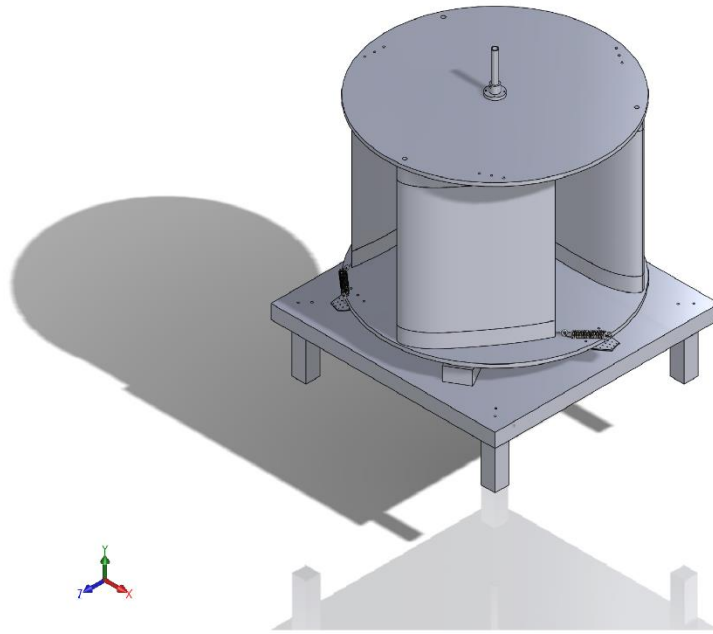


*Figure 14: CAD Model of design*

### 3.5 Initial Calculations

Once the final design of the turbine had been selected, initial calculations were done in order to predict the performance of the turbine.

When analyzing a wind powered turbine, a baseline wind speed area must be tabulated to use as an estimated wind speed for all calculations. To determine this value, the wind was sampled from Worcester over an entire year (2014) to obtain an average wind speed (weatherunderground.com). A distribution of the wind speed over the year can be shown in below in Figure 15.

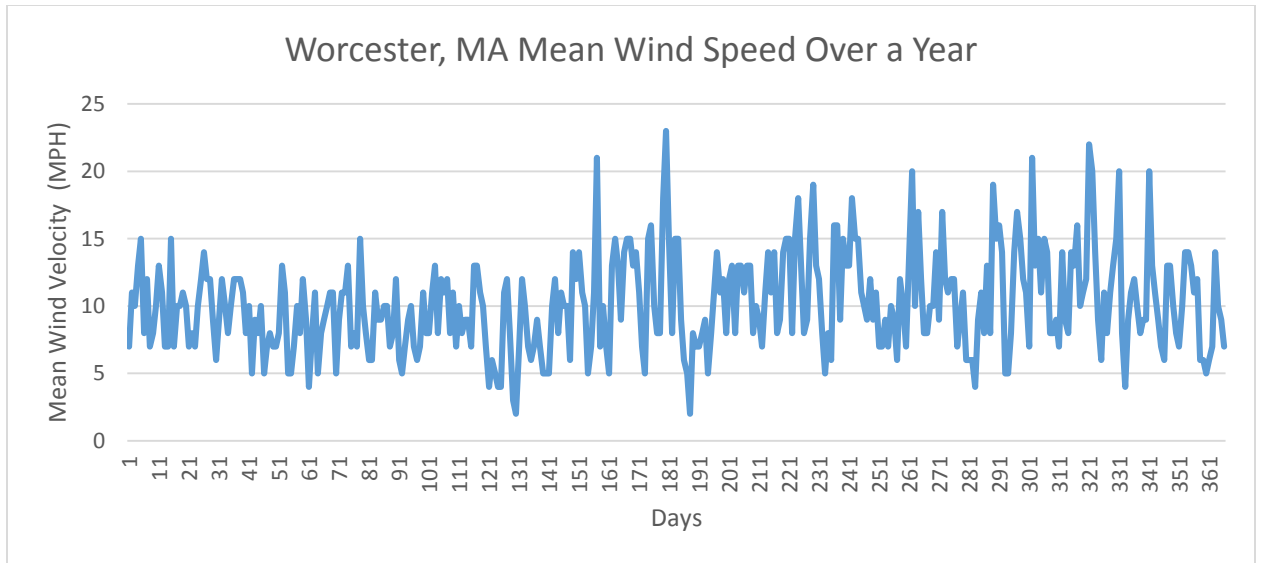


Figure 15: Mean Wind Speeds Over a Year

Weather Underground states that over an entire year, the average wind speed was calculated to be 10.20 miles/hour. The equivalent wind speed in meters per second is calculated below in Equation 3. The average wind speed in meters per second was calculated to be 4.50 meters/second. This wind speed value will be an approximate wind estimate to simulate the system in normal conditions.

$$Velocity \left( \frac{m}{s} \right) = Velocity (MPH) * 0.447$$

Equation 3: Velocity Conversion

Once the wind velocity (U) was calculated, numerical analysis could be conducted. For the proposed turbine, a square swept area (A) of 1 m<sup>2</sup> was assumed for the initial calculations. Based on Figure 6, a tip speed ratio (TSR) of 0.90 was assumed since the proposed design was closest in functionality to the Savonius wind turbine.

Equation 4 calculates angular velocity ( $\omega$ ) in radians/sec.

$$Angular Velocity = \frac{Tip Speed Ratio * Wind Velocity}{Radius of swept area}$$

Equation 4: Rotational Speed

From this equation a rotational speed of 46 RPM was calculated using the assumed values for area, wind velocity and tip speed ratio mentioned above. Using sea level air conditions, an air density ( $\rho$ ) was assumed to be 1.22 kg/m<sup>3</sup>. The coefficient of power (Cp) was assumed to be 0.15 for the team's designed wind turbine based on the Savonius properties in Figure 6 above.

Based on these assumptions, the ideal power that the turbine would be able to generate is calculated using Equation 5.

$$\text{Power Produced by turbine} = \frac{1}{2} * \rho * C_p * U^3 * A$$

*Equation 5: Ideal Power Produced*

A power of 8.30 W was calculated based on the 1 m<sup>2</sup> swept area. Using this power and the rotational speed, a torque produced can be calculated using Equation 6.

$$\text{Torque produced} = \frac{\text{power produced}}{\text{rotational speed}}$$

*Equation 6: Torque Produced*

The calculated torque was found to be 1.029 N\*m.

The purpose of doing the calculations above was to find what the power and torque of the wind turbine would be based on the area. Therefore, the calculations discussed above were done for a range of swept areas from 0.10 m<sup>2</sup> to 2.00 m<sup>2</sup>. Table 2 below shows a summary of the completed calculations.

Area (m <sup>2</sup> )	Radius (m)	TSR	Wind Velocity (m/s)	Omega (rad/sec)	RPM	Air Density (kg/m <sup>3</sup> )	Cp	Power (W)	Torque (N*m)
0.10	0.05	0.90	4.50	81.00	508.94	1.22	0.15	0.83	0.01
0.20	0.10	0.90	4.50	40.50	254.47	1.22	0.15	1.67	0.04
0.30	0.15	0.90	4.50	27.00	169.65	1.22	0.15	2.50	0.09
0.40	0.20	0.90	4.50	20.25	127.23	1.22	0.15	3.34	0.16
0.50	0.25	0.90	4.50	16.20	101.79	1.22	0.15	4.17	0.26
0.60	0.30	0.90	4.50	13.50	84.82	1.22	0.15	5.00	0.37
0.70	0.35	0.90	4.50	11.57	72.71	1.22	0.15	5.84	0.50
0.80	0.40	0.90	4.50	10.13	63.62	1.22	0.15	6.67	0.66
0.90	0.45	0.90	4.50	9.00	56.55	1.22	0.15	7.50	0.83
1.00	0.50	0.90	4.50	8.10	50.89	1.22	0.15	8.34	1.03
1.10	0.55	0.90	4.50	7.36	46.27	1.22	0.15	9.17	1.25
1.20	0.60	0.90	4.50	6.75	42.41	1.22	0.15	10.01	1.48
1.30	0.65	0.90	4.50	6.23	39.15	1.22	0.15	10.84	1.74
1.40	0.70	0.90	4.50	5.79	36.35	1.22	0.15	11.67	2.02
1.50	0.75	0.90	4.50	5.40	33.93	1.22	0.15	12.51	2.32
1.60	0.80	0.90	4.50	5.06	31.81	1.22	0.15	13.34	2.64
1.70	0.85	0.90	4.50	4.76	29.94	1.22	0.15	14.17	2.97
1.80	0.90	0.90	4.50	4.50	28.27	1.22	0.15	15.01	3.34
1.90	0.95	0.90	4.50	4.26	26.79	1.22	0.15	15.84	3.72
2.00	1.0	0.90	4.50	4.05	25.45	1.22	0.15	16.68	4.12

*Table 2: Hypothetical Turbine Calculations*

Based on the results from Table 2 above it was found that the bigger the turbine area, the more power and higher torque the turbine could output. Therefore the ideal turbine would have a swept area of 2 m<sup>2</sup>. However, based on the limitations of the manufacturing lab available to the team, the base diameter was constricted to 0.45 m (17.75 inches) in diameter. The cross sectional area was assumed to be 0.23 m<sup>2</sup>. This is explained in further detail in the construction section below.

Once the base plate circumference had been chosen the size of the airfoils were determined. The chord length of the airfoils were designed to be one sixth of the length of the circumference of the base plate in order to minimize flow interaction of the airfoils. The height of the airfoils were determined to be 0.457 m (18 inches) in order to maximize the swept area of the turbine without compromising the stability. Another reason for limiting the height of the airfoils would be to limit the inevitable imperfections occurring during manufacturing. Additionally, a height of 0.457 m allowed for the team to easily access the top of the turbine during testing and for the turbine to easily fit through doors.

Since the base plate diameter was selected to be 0.45 m in diameter, the table had to be larger than 0.45 m. One of the design specifications above also states that the turbine had to be portable i.e. fit through a standard door. Therefore the table had to be constructed to be larger than 0.45 m and less than 0.812 m.

## Chapter 4: Predictive Calculations

Once the sizing of the turbine had been determined the team made some predictive calculations in order to foresee how it would perform.

In order to predict the efficiency of the designed turbine, the team calculated possible power outputs for the fixed wing turbine to establish a base line of experimental expectations. The tip speed ratio,  $\lambda$ , is the ratio between the tangential velocity at the tip of the blade and the wind speed. This relationship is shown below in Equation 7. The tip speed ratio can be calculate experimentally or can be defined based on previously published experimental data.

$$\lambda = \frac{\omega R}{U}$$

*Equation 7: Tip Speed Ratio*

- Where  $\omega$  is the rotational speed in radians per second
- R is the turbine radius in meters
- U is the wind speed in meters/second

The tip speed ratio is used to show the relationship between the wind velocities and how fast the turbine is rotating and is an important factor used to classify turbines.

The fluid velocity, in this case the wind velocity, acting on each blade varies at different points of the rotation. Theta,  $\theta$ , is the location of the blade in its orbit around the axis. Maximum oncoming fluid velocity is at  $\theta=0^\circ$ , minimum oncoming fluid velocity is at  $\theta=180^\circ$ . Using theta and the tip speed ratio it is possible to determine resulting wind velocity and the angle of attack that the airfoil sees as it rotates. These relationships are diagramed in Figure 16 below.

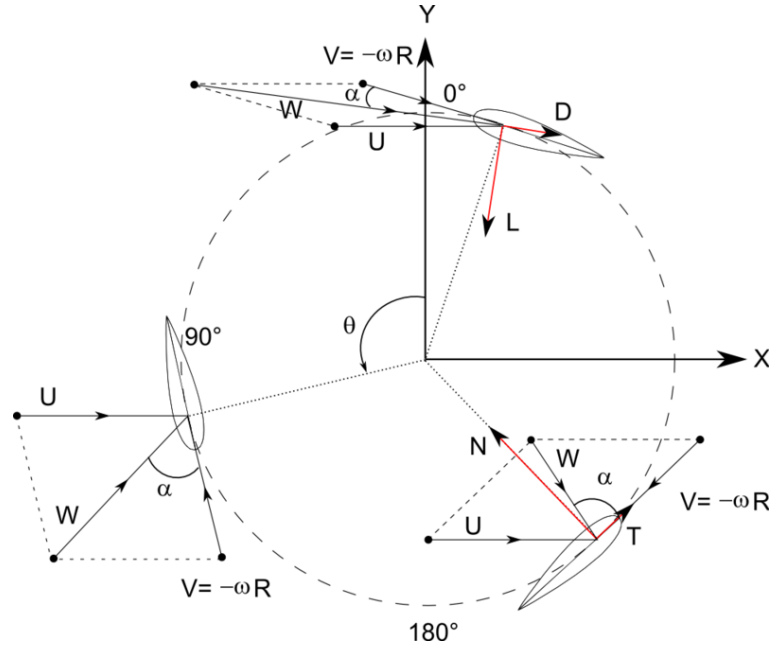


Figure 16: Forces and Velocities Acting on a Vertical Axis Wind Turbine

The resulting velocity,  $W$ , is the blade velocity relative to the turbine and can be found using Equation 8 below

$$W = U\sqrt{1 + 2\lambda\cos\theta + \lambda^2}$$

Equation 8: Resulting Velocity

The angle of attack  $\alpha$ , can be found using Equation 9:

$$\alpha = \tan^{-1}\left(\frac{\sin\theta}{\cos\theta + \lambda}\right)$$

Equation 9: Angle of Attack

The angle of attack is used to find the coefficient of lift and coefficient of drag from the experimental data seen in Chapter 3.3. The lift and drag coefficients are then used to calculate the power output of the turbine. Lift and drag can be found using Equation 1 and Equation 2 found in chapters 2.2.1 and 2.2.2. The coefficient of lift and drag can be found from Figure 10 and Figure 11 in chapter 3.3. Once the lift and drag forces are found, the resultant force must be identified. The resultant force is based on the relationship between the lift and the drag. This is shown below in Equation 10.

$$\vec{R} = (D_x + L_x)\hat{i} + (D_y + L_y)\hat{j}$$

Equation 10: Resultant equation

Where the sum of the x components of the lift and drag equals the x component of the resultant force. The resultant force is used to find the torque. The torque is equal to the perpendicular force applied across a lever arm. For this turbine the lever arm is the

distance from the attachment point to the axis of rotation (the radius). In this case it is  $R_x$ , the resultant force in the x direction. Torque is needed for the power equation derived from Equation 6 in chapter 3.5 shown below in Equation 11.

$$Power = Torque * Omega$$

*Equation 11: Power Equation*

Due to the fact that there are three blades, the total power includes the power generated by all three blades as they move around the axis. The three airfoils are placed equally around the axis, therefore  $\theta=0, 120, 240$  are the angle positions of each airfoil for phase one and  $\theta=60, 180, 300$  are the positions for phase two. Each phase references the location of the three blades. Phase two is a 60-degree rotation after phase one. Using the equations outlined above, and setting the variables at values in Table 3 below, predicted power values were calculated for the fixed wing turbine. The detailed calculations are shown in Appendix B.

Variable	Value	Unit
Omega	39.37	rad/sec
Radius	0.23	meters
Tip Speed Ratio	0.90	(unitless)
Chord Length	0.24	meters
Height	0.46	meters
Area (Chord*Span)	0.11	m <sup>2</sup>
Density	1.23	kg/m <sup>3</sup>

*Table 3: Predictive Power Calculation Variables for Fixed Turbine*

The velocity was iterated between 5 m/s and 10 m/s in 0.5 m/s increments to predict the power that the fixed blade turbine would produce. For these predictions, ideal, no friction, and constant wind velocity conditions were assumed. The results for the power calculations are summarized in Table 4 below.

Wind Speed (m/s)	Power (W)
5.00	3.07
5.50	4.09
6.00	5.31
6.50	6.75
7.00	8.43
7.50	10.37
8.00	12.59
8.50	15.10
9.00	17.93
9.50	21.08
10.00	24.59

Table 4: Predicted Power at Different Wind Speeds

The results from Table 4 are plotted in the power vs wind speed graph shown in Figure 17 below.

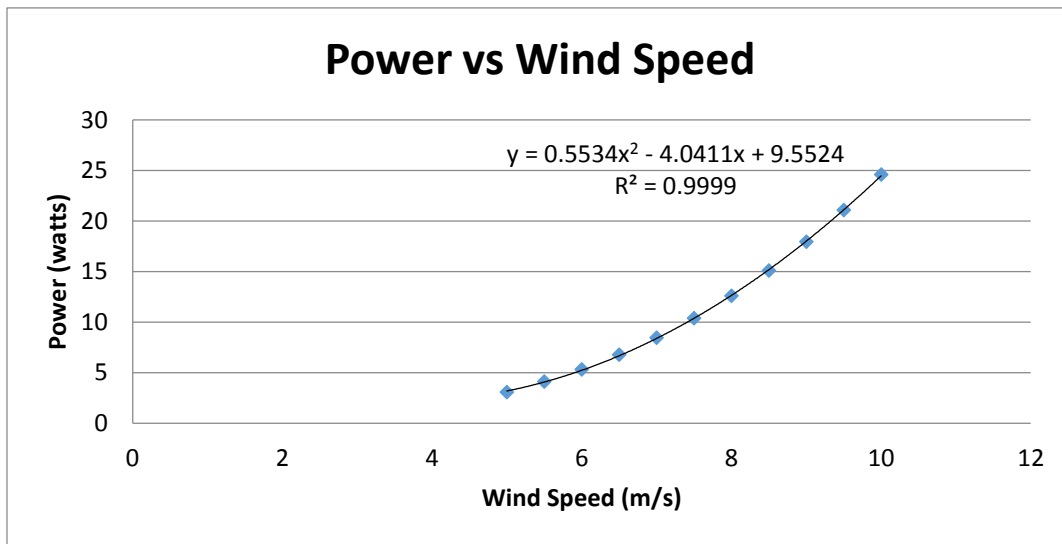


Figure 17: Calculated Power vs Wind Speed graph

The trend line shown in Figure 17 is what the team expected to see based on research in other turbines where the same curved line of best fit was observed. The data is a second order polynomial, and demonstrates an ideal prediction of the power the turbine is capable of producing in a fixed blade system.

## Chapter 5: Construction

Once the final design had been chosen and the dimensions were finalized, construction of the turbine commenced. Below is a detailed description of the team's manufacturing process of each section of the turbine. The base was completed first, followed by the prony brake, airfoils and associated connecting hardware.

### 5.1 Base

The base of the turbine was constructed using easily accessible and cost effective materials: wood and nails. For the counter top, an old table top was cut into the desired dimensions. This reused table top was chosen for the group's purposes since it was level, had adequate structural sturdiness, and the composite countertop material was easy to work within the construction phase. These features were of high importance in order to meet the MQP team's design goals.

The table was chosen to be approximately 31x31x31 inches. The height was chosen to allow sufficient access to the prony brake, which was located under the table. The width and depth of the table were required to be in the range of 18 to 32 inches. Therefore the width and depth of the table were arbitrarily chosen to be 31 inches since it allowed for the 18 inch diameter airfoil plate to fit on the table and it was small enough to easily fit through a standard door of 32 inches.

Once the table top was cut to the appropriate dimensions, the center of the table top was found and a 1.5 inch diameter hole was made at this center point. The dimension for this hole was chosen to ensure that there would be no interference between the 0.9 inch diameter shaft and the table top.

The table was constructed with four legs each made using two 2 x 4 x 30 inch pieces of wood. The two pieces were attached using six 2.5 inch long screws. Wooden 2 x 4 pieces were used since they were economical; two of them were attached to make each leg in order to ensure structural stability. It was also important that the table was made to be as level as possible. Three screws were used on each side, spaced as shown in Figure 18 below. The three screws on the opposite side of the leg were placed such that the screws alternated sides along the leg.



Figure 18: Screw placement for table leg

A supporting frame was constructed to ensure structural stability of the table. This frame consisted of two 2 x 4 x 30.5 inch pieces of wood and two 2 x 4 x 27.5 inch pieces of wood. These pieces were attached to make a square shape around the outer perimeter of the table top as seen in Figure 19 below. This frame was attached to the table top using two screws in each corner and one screw along each length of the square perimeter; 3 inch length screws were used.



Figure 19: Supporting frame of table

Once the supporting frame was built and attached, the legs were attached to the table top. The legs were placed on the inside corners of the supporting frame as seen in Figure 19 above. Each leg was attached to both the table top and the supporting frame using the 2.5 inch screws. It was attached to the frame using two screws per leg, two on each corner. Two screws were also used to attach the plate to the legs. The placement of the screws was such that each screw attached to different 2 x 4 inch pieces of wood. The attachment of the legs is shown below in Figure 20.

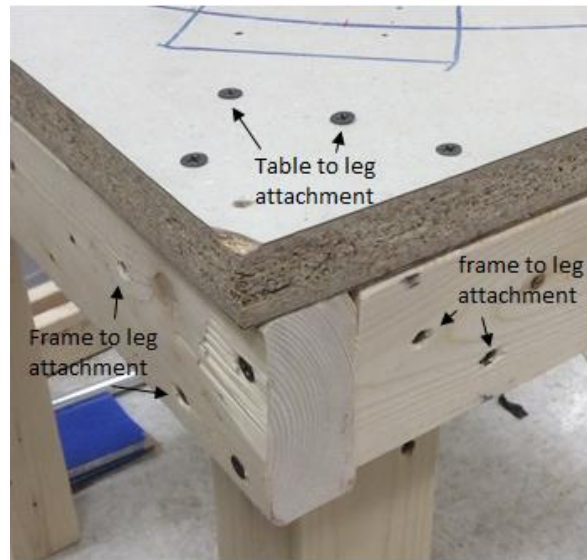
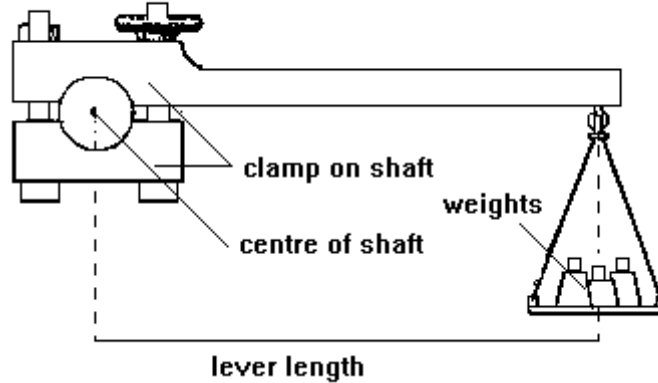


Figure 20: Leg attachment

## 5.2 Prony Brake

One of the main experimental measurements of this project is the torque produced by the system. In order to measure this, a prony brake was investigated. This system employs the use of a cantilever arm with length  $L$  with a weight attached onto the end. This cantilever arm clamps onto the main drive shaft. Once the shaft starts to move, the clamp is tightened onto the main shaft until the cantilever beam is balanced in a horizontal position. The weight that is on the end of the cantilever has a specific force ( $F$ ). An example of this system is shown below in Figure 21.

### 9.2.19 Prony brake



*Figure 21: Prony Brake*

Before constructing the prony brake, research was done to find examples which other people had already constructed and tested. Several examples were found of homeowners using them for various purposes. Figure 22 below shows one homeowner's assembled prony brake onto an engine.



*Figure 22: Example prony brake*

The initial problem faced with the prony brake was that the motion which the turbine was outputting was vertical rotation. However for the prony brake to function, horizontal rotation was required. This horizontal frame of motion was required since the prony brake uses the gravitational force to operate. Therefore, a right angle translation piece was attached to the bottom of the turbine shaft. The prony brake would then be attached to the piece at the other end of the angle adjustment piece seen in Figure 23 below.



*Figure 23: 90 degree angle motion adjustment*

The prony brake itself was constructed from a 0.75 x 2.5 x 30 inch piece of wood. The final product is seen in Figure 24 below. The length of the long arm was cut to be 21 inches and the bottom piece was 5 inches. The hole seen at the center of the long arm and the bottom piece was cut to be 5/16 inches in diameter. This dimension was chosen due to the size of 90 degree angle adjustment piece which was 6/16 inches. The hole diameter was slightly smaller than the diameter of the angle adjustment piece so that the prony brake could clamp onto the attachment point. The wing nuts were chosen so that the tightness of the prony brake could be easily adjusted during testing without dependency on tools. The hook on the right end of the brake is in place to attach the prony brake to the Vernier force gauge. The constructed prony brake is shown below in Figure 24, Figure 25, and Figure 26.



*Figure 24: Constructed prony brake*

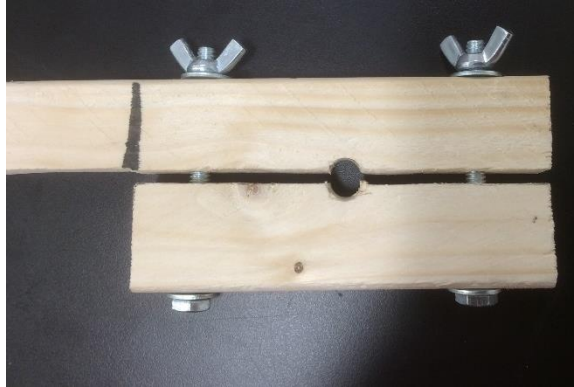


*Figure 25: Loose prony brake head*

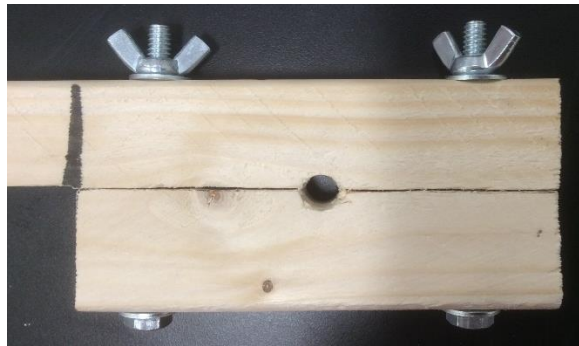


*Figure 26: Tightened prony brake head*

### 5.3 Airfoil plates

Once the base and the prony brake were constructed the team moved on to the head of the turbine. First the team constructed the two circular airfoil plates which were 17.7 inches in diameter, made of plexiglass and were cut using a Versalaser VLS. Lasercutter. The laser cutter used DWG files and cut the plexiglass to the desired shape within an 18 inch by 24 inch cutting frame. The hole at the center of the plate was laser cut to be 1 inch in diameter, slightly larger than the shaft diameter to ensure some clearance space to minimize interference. Four holes of diameter 0.128 inches were made on the plate for the collar attachment piece. The collar attachment piece was used to connect and translate the motion from the airfoils to the shaft. The other six holes seen on the outer part of the plate are all 0.25 inches in diameter used for attaching the airfoils. The SolidWorks file used to laser cut the plates can be found in Appendix C. A cut airfoil plate is shown below in Figure 27.

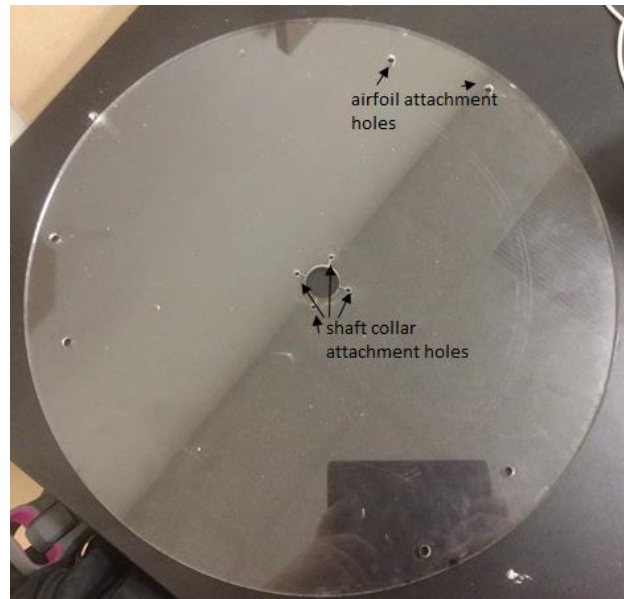


Figure 27: Airfoil plate

#### 5.4 Ball bearings

The ball bearings seen in Figure 28 below were used to allow the airfoil plate to rotate with minimal interference. Extra grease was used to minimize the friction on the ball bearings. The four ball bearings were spaced equally around the circumference of the plate. Four ball bearings were chosen to be used to maximize stability. They were attached to pieces of wood which were 2.5 inches in height, which were then attached to the table plate. These wooden blocks were used to create clearance space between the table plate and the airfoil plate.



Figure 28: Ball Bearing

#### 5.5 Airfoil plate attached to the base

Once all the individual parts were assembled, the airfoil plate could be attached to the shaft and the base. The collar seen in Figure 29 below was used to attach the shaft to the

top and bottom airfoil plates. Using electrical tape, the shaft, and collar were made flush with each other. Then a bolt was attached through the collar and shaft to limit movement relative to each other. This ensured that the motion would be translated between the airfoils and the plates with minimal efficiency loss.



*Figure 29: Shaft attachment collar*

## 5.6 Airfoil Construction

Next the three NACA 2412 airfoils were made. The airfoils were built over a two month span with the main components being dense foam and plywood. Particular preparation and various adhesives allowed the airfoils to take their final shape and allowed for the turbine to output power. The concept behind the construction of the airfoils was to cut the foam into 2 inch thick profiles, stack those profiles to the desired height, and add plywood tops and bottoms. The plywood was added to allow strength where the airfoils are attached to the plexiglass. Glue, nails, and bolts were used as adhesives between the airfoils, wood, and plexiglass.

All of the foam was cut using a Manix Hot Wire Cutter. The hot wire cutter allowed precise cutting of the foam with a medium temperature and a constant slow speed. All of the plywood was cut with the laser cutter. The foam was initially prepared by cutting it into 3 x 11 x 2 inch blocks so that the individual airfoils could be easily handled and cut to the desired approximately 2 x 9 inch profile as above in Figure 12.

After several attempts, it was found that the best way to cut the airfoils was to use wooden profiles on the top and bottom of the foam and let the hot wire cutter run against the wood to get a precise cut. The profiles were made using 0.25 inch plywood. Three holes were drilled on each of the plywood profiles where screws would be placed later to hold the wooden profiles onto the foam in order to prevent unnecessary movement. A drill-bit was used to drill holes in the foam in order to allow ease of screw attachment to the foam at a later time. In order to attach the wooden profiles and the foam, screws were then driven through the profile, through the foam and through the second profile on the other side of the foam. The pictures seen in Figure 30 and Figure 31 below demonstrates the cutting technique and the plywood screw support respectively.

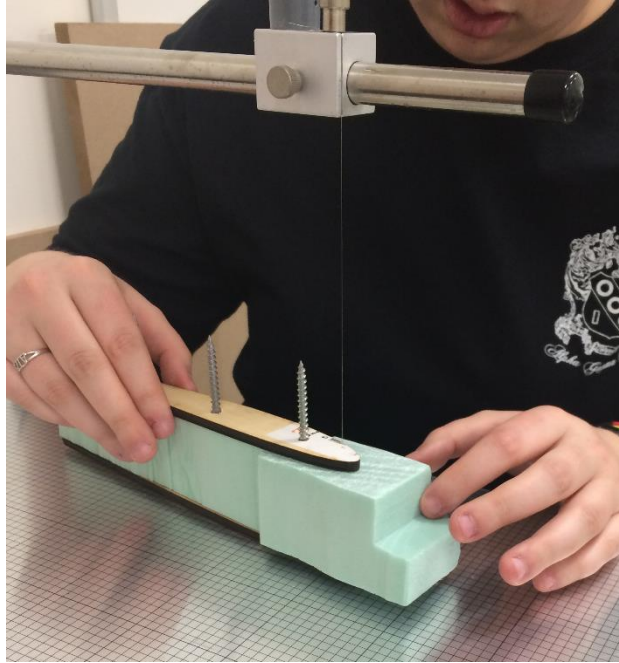


Figure 30: Cutting technique with the Manix Hot Wire Cutter

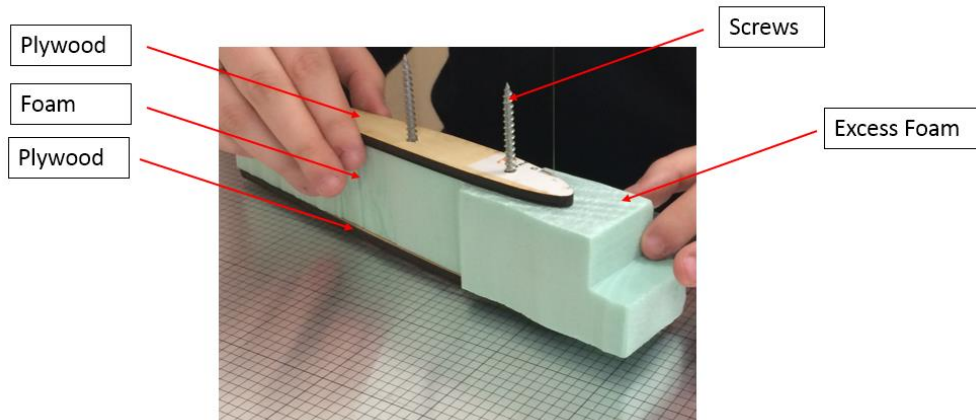


Figure 31: Plywood and screw supports used to align the foam

A total of four 2 inch profiles were cut and were then glued on top of one another using regular wood glue to create a total of 3 airfoils. In order to make sure the foam pieces did not move while the glue was drying, they were nailed together temporarily. After a day the nails were removed and the resulting holes were plastered over to make a smoother profile.

Wooden profiles were attached at the top and bottom of each airfoil, which allowed for a firm surface to attach the airfoils to the base. These wooden profiles consisted of four 0.25 inch thick plywood profiles that had two 0.628 inch holes cut into them for attachment purposes and one 0.25 inch profile with no holes in it. The five profiles were

glued together using the same wooden glue which was used for the foam stacking. The holes in the pieces of wood were vertically aligned so that the airfoil could be attached to the plexiglass. The 0.25 inch profile with no holes would be placed between the other wooden profiles and the foam profiles. The alignment of the holes is shown below in Figure 32.

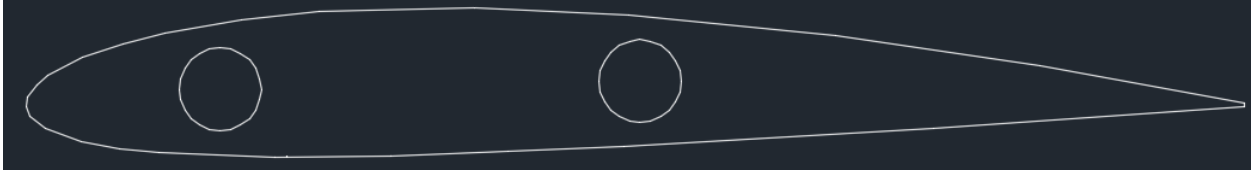


Figure 32: Placement of the 5/8" holes on Airfoil

The final placement of the wood end pieces are shown below in Figure 33.

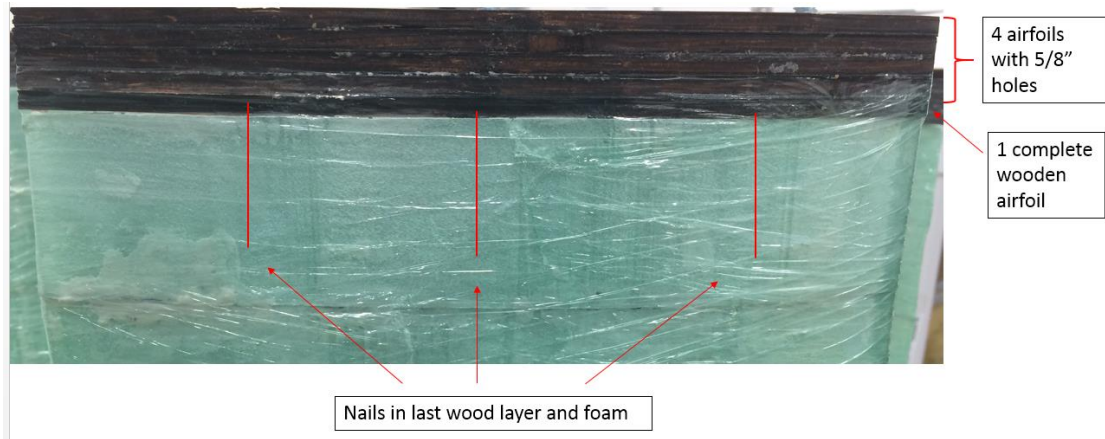


Figure 33: Wooden profile and the location of nails

Three holes were then drilled into the completed profile; these holes were used to attach the profile and foam using nails. Wood glue was also used to attach the foam and profile, since using only one attachment method did not result in an adequately stiff attachment. Wood glue was applied to the nails as well as on the surfaces to fully constrain the airfoil. This process was repeated for the top and bottom of all 3 airfoils. A completed airfoil is shown below in Figure 34.



*Figure 34: Complete airfoil*

In order to limit friction between the bolts and the wood, plywood spacers were glued into the 0.628 inch holes of the wooden profiles. The nylon and plywood spacers allowed the 0.25 inch bolt to sit in them and rotate freely while allowing limited translational movement. The nylon spacers were 0.375 inches thick and were used in conjunction with 0.25 inch plywood spacers. This was done due to economic reasons, since plywood is cheaper and the spacers could be manufactured using the laser cutter and wood glue. The drawback to the wooden spacers, and the reason why both were used, is that the nylons spacers had less friction, however, they would not stay fixed to the airfoil.

The bolts were then attached to the plexiglass plate in the holes seen in Figure 27 above, which allowed the airfoils to sit on the bolts. This allowed for complete rotational movement.

### 5.7 Spring Attachment System

The spring attachment system on this device allows for the articulation of the airfoils. On the trailing edge of each of the airfoils there is an eyehook that is screwed into the bottom of the airfoil as shown below in Figure 35.



*Figure 35: Eyehook attachment*

Once these hooks were added, the spring attachment plates were laser cut out of acrylic. These plates included three holes for bolting the spring attachment plate on the base plate and a matrix of holes for the eyehook attachment. This matrix of holes allow for adjustable angles of the spring. Plates were attached behind the trailing edge of each airfoil and the three plates spaced 120 degrees apart from each other. The spring attachment piece is shown installed below in Figure 36.

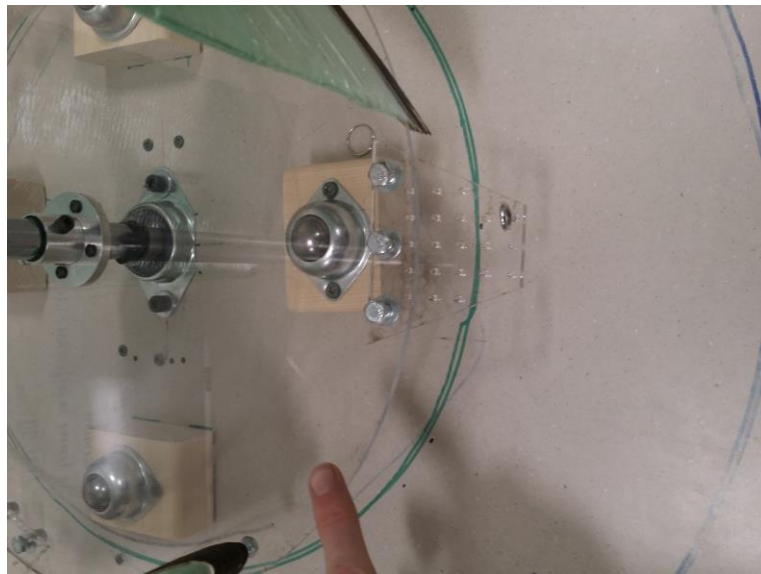


*Figure 36: Spring Attachment Piece*

Finally, the springs were connected from the eyehooks on the bottom of the airfoil to the eyehooks screwed into the spring attachment plate. Key ring loops were used as an intermediary connection between the spring and the eyehooks. This configuration is shown below in Figure 37.

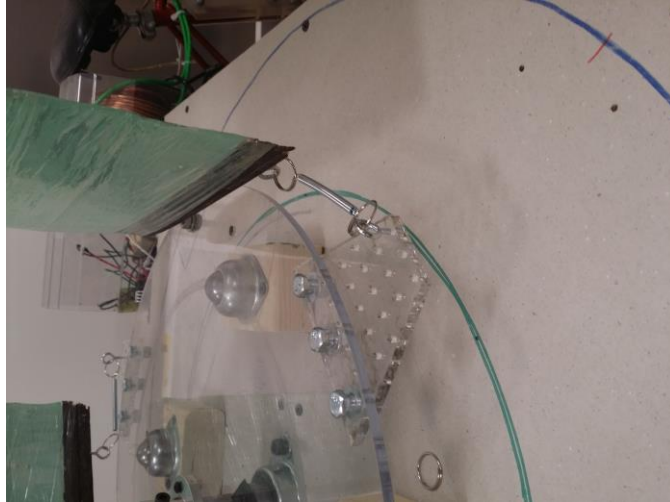


*Figure 37: Final spring configuration*

## Chapter 6: Testing

There were three key phases to the turbine testing: proof of concept, RPM, and torque testing. Proof of concept testing was used to determine if the turbine could operate and to gain an understanding of what wind speeds were required for operation. RPM testing was used to observe the relationship between the wind speed and RPMs while torque testing measured the wind speed and calculated the force generated using the prony brake. The team conducted testing at two different locations over the course of a three week period. This was due to the variation of the wind in the form of wind gusts. The first location was done on the WPI Campus in the area between Higgins Laboratories and Alumni Gymnasium. This location was chosen due to the higher wind speed velocities compared to the rest of campus. The second testing location was Worcester Regional Airport which was located on a large flat hill in Worcester, MA. At this location, the team conducted the RPM and torque phases due to the lack of consistent wind velocities at the WPI Campus. Due to the inconsistency of the wind, the team was forced to conduct the different phases of testing non-sequentially.

### 6.1 Phase I: Proof of Concept

The first phase was the proof of concept testing. This testing was used to determine which designs worked. During this phase the team also confirmed the most appropriate testing locations. All design tests were done without the prony brake and right angle transmission piece to lower the starting torque. The test procedure was to setup the turbine, monitor the wind speeds, and observe if the turbine was able to operate. If the turbine rotated the design moved onto the next phase of testing. If the turbine did not rotate, one of two decisions were made. If the location did not experience high enough wind speeds, determined to be 10 m/s (22.4 mph), then the turbine was moved to a different location or testing was suspended until a later time. If the area did experience wind speeds of at least 10 m/s and the turbine did not spin then the turbine failed the proof of concept testing and did not advance to the next phase. The maximum wind speed observed during testing was recorded in order to understand the range of air speeds required for operation.

### 6.2 Phase II: RPM Testing

The second phase of testing measured the RPMs of the turbine and the observed correlating wind speed. This testing was conducted in a location that had passed proof of concept testing. One individual recorded the turbine motion with a camera and a second individual measured the wind speed in the area. To record the RPMs, one of the airfoils was given a blue stripe to make it identifiable in the video and therefore easier to count the revolutions. The person recording the wind speed would state the observed wind speed every 5 seconds so that it could be recorded by the video. The testing footage was then observed and later transcribed to evaluate the wind speed and RPMs. During testing

the turbine would typically spin for 10 to 20 seconds; the average wind speed during that span was taken and the RPMs were counted on the turbine.

### 6.3 Phase III: Torque

The third phase of testing was focused on the collection of force data, which would then be used to calculate the torque of the turbine. All force testing was done at Worcester Regional Airport due to more consistent wind speeds compared to WPI's campus. A Vernier force gauge was pinned onto the side of the base and used to measure the force produced by the turbine as the prony brake was attempted to rotate downward as seen in Figure 38 below. Before each test, the Vernier was zeroed while the turbine was manually stopped with no force being applied to the gauge. Using Logger Pro software, the Vernier force gauge measured the observed force over a 120 second span. During this time, the wind speeds were manually observed and recorded every 20 seconds. Using the time scale on the produced graph, the wind speed points were then matched up with the corresponding force to produce a plot that demonstrated the torque to wind speed relationship. This was done five times in order to obtain a large sample size between wind speeds and the torque produced by the turbine.



*Figure 38: Vernier Force Gauge Testing Set Up*

## Chapter 7: Results

The team was successful in collecting data over a three-week period of time in separate testing sessions. Due to the behavior and variance of the wind, the team was unable to collect a consistent number of data points in each testing session. This resulted in 9 points of data for RPM testing and 31 data points for torque testing. The difference is due in part to the fact that during the RPM testing, the team manually recorded data while the torque data was collected by a digital output.

### 7.1 Phase I: Proof of Concept

The initial proof of concept test determined whether or not the turbine rotated when the airfoils were articulating and not articulating. The articulating test was initially done with the leading bolt fixed and the trailing bolt unfixed, leaving the trailing edge of the airfoil to move freely. This resulted in the turbine beginning to spin at an initial speeds ranging from 6 to 7m/s. The non-articulating turbine had both bolts on all three airfoils fixed which constricted the airfoils movement. The non-articulating turbine experienced wind speeds of at least 12 m/s (26.8 mph) and did not spin; therefore it failed the proof of concept testing as summarized in Table 5.

Turbine	Did it start spinning?	Minimum Wind Speed to Start
<b>Articulating</b>	Yes	6 m/s
<b>Non-Articulating</b>	No	12 m/s (did not spin)

Table 5: Phase I Table

#### 7.1.1 Starting Torque

During phase I, the team noticed that there was a delay for the turbine to start rotating. Therefore the team calculated how much time of steady wind velocity was required for the turbine to start rotating. This was done by integrating the angular velocity with respect to the calculated angular acceleration; this integration is shown in Appendix D.

The first step in finding the time required to start the turbine was to find the torque required to overcome the static friction. This was done by attaching the Vernier force gauge to the top plate of the turbine. The Vernier force gauge recorded the force the turbine overcame as it initially started to rotate. This initial force was found to be 1.12 N which translates to a starting torque of 0.25 N\*m as explained by Equation 6.

In addition to the initial torque of the turbine, the torque output at winds of 6 m/s was measured. This was done by attaching the force gauge to the prony brake on the turbine; this method is explained in detail in chapter 7.3. From the data collected it was found that at 6 m/s wind speeds the turbine was outputting 0.53 N\*m of torque.

The next step was to find the moment of inertia of the turbine. This was done by making a SolidWorks model of the turbine, as seen in Appendix D. The moment of inertia was calculated to be 0.40 kg\*m<sup>2</sup>.

Once these values were found the team solved for the angular acceleration (a) of the turbine to reach observed RPM values at 6 m/s wind speeds. This was done using the relationship shown in Figure 12 Equation 12 below. An angular acceleration of 0.70 rad/s<sup>2</sup> was found.

$$\text{Torque} - \text{Frictional Torque} = \text{Inertia} * \text{Angular Acceleration}$$

*Equation 12: Torque, Inertia, and Angular Acceleration*

During testing, the team observed that sustained winds of 6 m/s, over a unit of time, was required for the turbine to start rotating. The turbine also had to rotate approximately 120 degrees ( $\theta$ ) in order for two of the airfoils to catch the wind and begin to articulate, once this occurred the turbine would begin rotating from Equation 13 below, the team calculated the minimum time of constant wind speed required for the turbine to start. The calculation from Equation 13 showed that the turbine required 2.4 seconds of constant wind in order for the turbine to start rotating.

$$\theta = \frac{1}{2} * a * t^2$$

*Equation 13: Rotation, time and acceleration*

## 7.2 Phase II: RPM Testing

In the second phase of testing, the team looked at the correlation between wind speed and RPM. The data summarized in Table 6 and Table 7 below was obtained from the RPM testing. The data was separated into two tables for ease of viewing. The rows represent the wind speed measured in m/s, the RPM, and the angular velocity of the turbine. The wind speed and RPMs were observed while the angular velocity was found using Equation 14 below.

$$\omega = \frac{\text{RPM} \times 2 \pi}{60 \text{ sec}}$$

*Equation 14: Angular Velocity Calculation*

	WPI Campus 1	Airport Testing 1	Airport Testing 2	Airport Testing 3
<b>Wind Speed (m/s)</b>	8.4	5.5	6.5	6.8
<b>RPM</b>	80.0	52.5	60.0	65.0
<b>Angular Velocity (Rad/s of turbine)</b>	8.3	5.5	6.2	6.8

*Table 6: Phase II RPM wind speed Table (1)*

	Airport Testing 4	Airport Testing 5	Airport Testing 6	WPI Campus 2	WPI Campus 3
<b>Wind Speed (m/s)</b>	9.5	9.0	8.5	12	10.7
<b>RPM</b>	96.0	75.0	63.0	79.2	76.3
<b>Angular Velocity (Rad/s of turbine)</b>	10.0	7.8	6.5	8.3	7.9

*Table 7: Phase II RPM wind speed Table (2)*

As is seen from Table 6 and Table 7, the team found that the RPMs ranged from 52.5 to 96.0 RPMs. The testing results above led to the following graph, Figure 39, which shows the relationship between wind speeds and RPM.

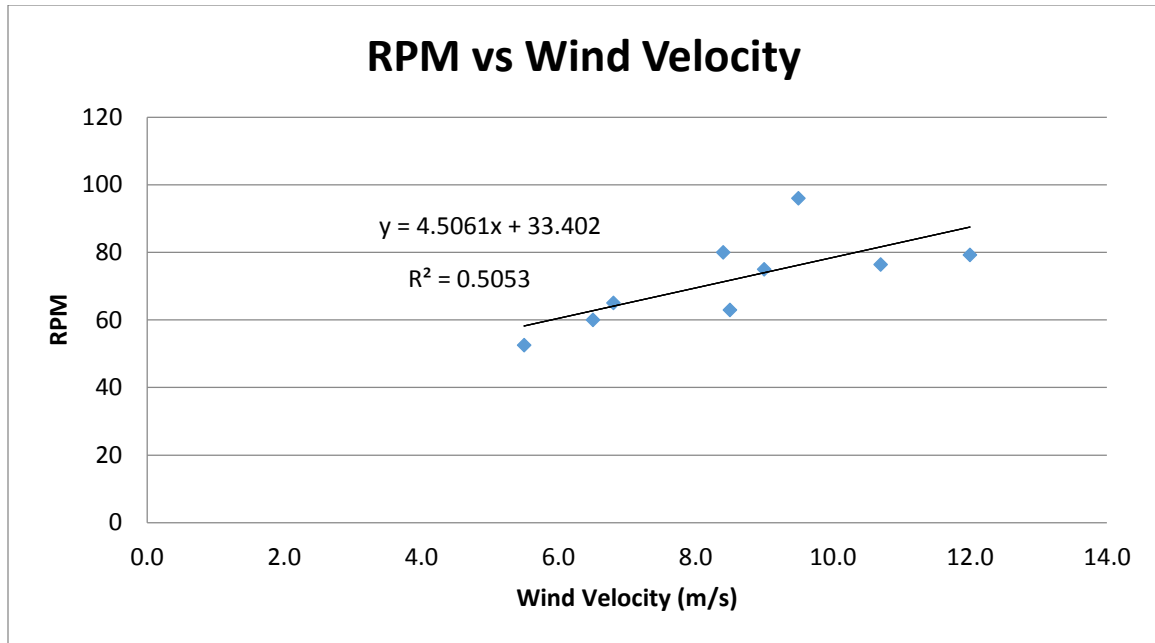


Figure 39: RPM to Wind Speed

As expected, the team found the relationship between RPMs and Wind Speed to be positive and linear. This is due to the angular velocity's relationship with linear velocity given a constant radius R. This relationship is shown in Equation 15.

$$\omega = \frac{U}{R}$$

Equation 15: Angular Velocity

As was expected, the RPMs of the turbine increased as the wind speed increased because the tip speed ratio shows that the driving factor affecting the speed of the turbine is the speed of the wind. As is seen in the graph shown in Figure 39 above, an equation for the line of best fit shows the relationship between RPM and wind speed based on the nine data points, which is summarized in Equation 16. The team determined that Equation 16 below is only applicable for wind speeds of 5 to 12 m/s as the relationship cannot be extrapolated because the turbine does not start until 6 m/s wind speeds are observed. Given this observed information, the team expected a RPM value of zero for the wind speeds between 0 to 5 m/s. With this relationship the team determined that the RPM to wind speed relationship is best defined as a piecewise function where from 0 to 5 m/s the turbine has no RPMs and from 6 to 12 m/s the relationship is best described by Equation 16:

$$RPM = 4.51 \times U + 33.40$$

Equation 16: RPM Correlation

### 7.3 Phase III: Torque Testing

The third and final phase of testing measured the approximate torque produced by the turbine. This was done using the Logger Pro Software. The team collected the force acting on the force gauge over an interval of 120 seconds which was then plotted against time. An example of the data collected is shown in Figure 40 below. Four torque test graphs similar to Figure 40 were also recorded and can be found in Appendix E.

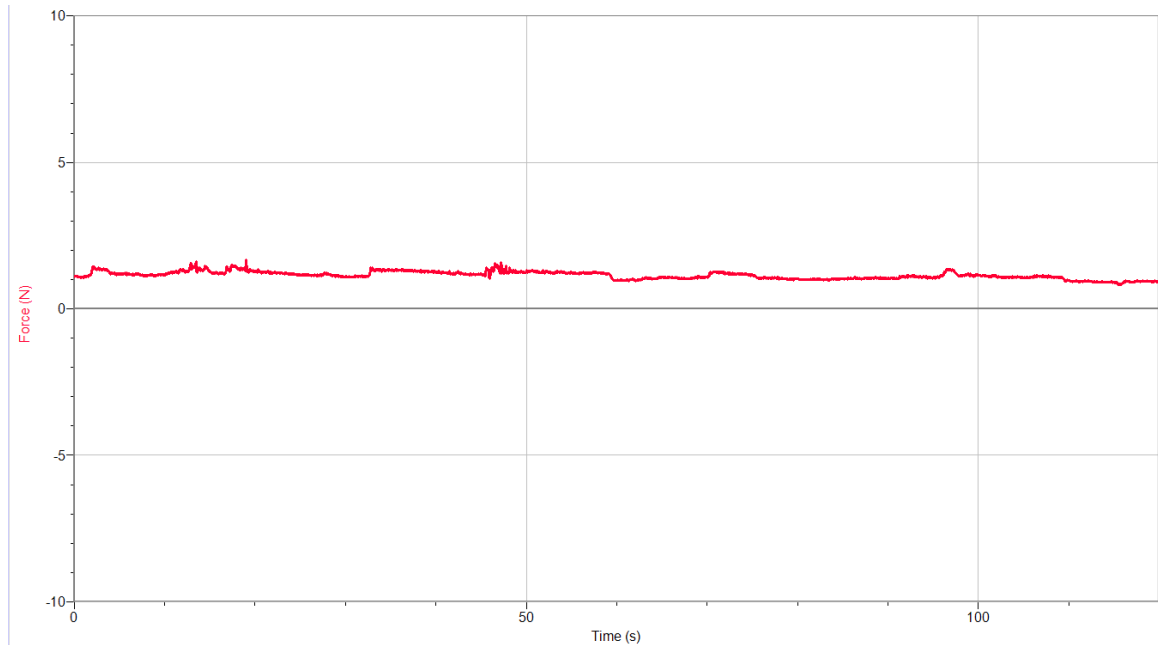


Figure 40: Torque Testing

For the test conducted resulting in Figure 40 the wind speed was recorded at 20 second intervals. As is seen in Figure 40 the force was continuously recorded by the Vernier force gauge. The team specifically recorded the force at each 20 second interval so that the torque could later be calculated and associated with a specific wind speed. This is summarized in Table 8 below. Appendix D shows similar tables of results for each of the four torque testing result graphs.

Seconds	Wind Speed (m/s)	Force (Newton)
20	7.2	1.275
40	7.8	1.233
60	7.0	0.969
80	6.5	1.017
100	6.8	1.131
120	5.0	0.915

Table 8: Lever Arm Calculation

Using the force data from the table above and the relationship between force and torque shown in Equation 17 below the team calculated the torque of the turbine. In Equation 14 Equation 17, the 0.469 meters is the length of the prony brake's lever arm measured in meters.

$$\text{Torque} = \text{Force} \times 0.469$$

Equation 17: Prony Brake Torque Calculation

The team then plotted all data from the five tests to produce a torque to wind speed plot shown below in Figure 41.

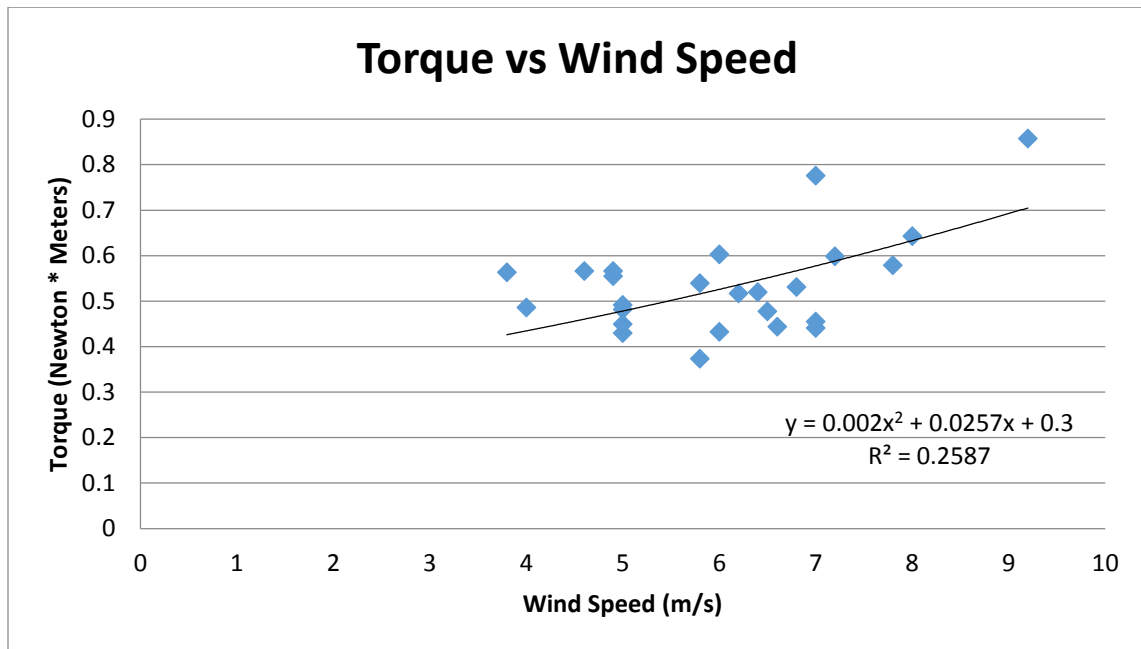


Figure 41: Torque vs Wind Speed

In the figure above, the line of best-fit shows that the relationship between wind speed and torque to be a curve as expressed in Equation 18.

$$\text{Torque} = 0.002U^2 + 0.0257U + 0.3$$

Equation 18: Torque Wind Speed Relation

While the  $R^2$  shows the equation being 25% correct, this trend line is promising as the relationship between torque and wind speed should be quadratic as is seen by the algebraic evaluation of the units. The results do not clearly show a quadratic relationship because of the small sample size of the data.

The turbine was able to produce between 0.37 to 0.86 N\*m of torque at wind speeds from 3.8 to 9.2 m/s. At higher velocities the quadratic nature of the data should become more apparent. From the uncertainty of the curve, the team does not believe the data can be extrapolated to predict the torque at winds speeds less than 3.8 m/s or more than 9.2 m/s.

Using the tests that were executed, the team was unable to observe the relationship between torque and RPMs directly. By analyzing the data collected the team was able to make the assumption that a RPM and torque collected at different times, but at the same wind speed are related.

Using the assumption mentioned above, the team was able to find three concurrent wind speed points that possessed unique RPM and torque values. These points are shown below in Table 9.

Wind Speed (m/s)	Force (N)	Torque (N*m)	Wind Speed (m/s)	RPM
6.5	1.02	0.48	6.5	60
6.8	1.13	0.53	6.8	65
9.3	1.83	0.86	9.3	96

Table 9: Wind Speed, RPM and Torque

The team then plotted the points from Table 9, on the torque versus RPMs graph shown in Figure 42 below. Using a line of best fit, the team determined the approximated relationship between torque produced and RPMs generated.

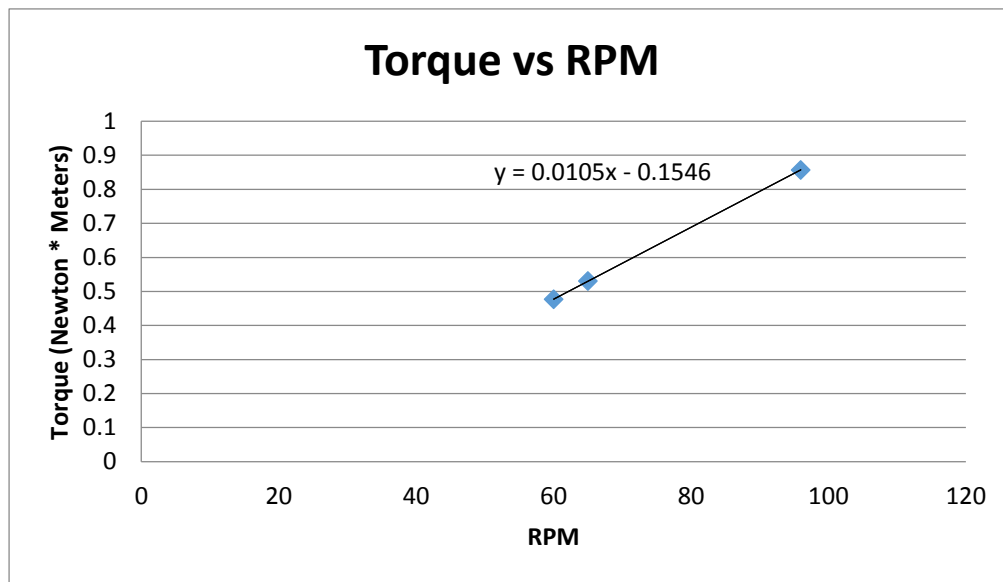


Figure 42: Torque vs RPM

From the line of best fit, the relationship between torque and RPM is summarized in Equation 19 below.

$$Torque = 0.0105 * RPM - 0.1546$$

Equation 19: Derived Torque vs RPM

Using the relationship in Equation 19, the team then populated a graph of torque against RPMs using all of the recorded data points. From all collected RPM data, a torque

was found using Equation 19 and vice versa. The resultant plot is shown below in Figure 43.

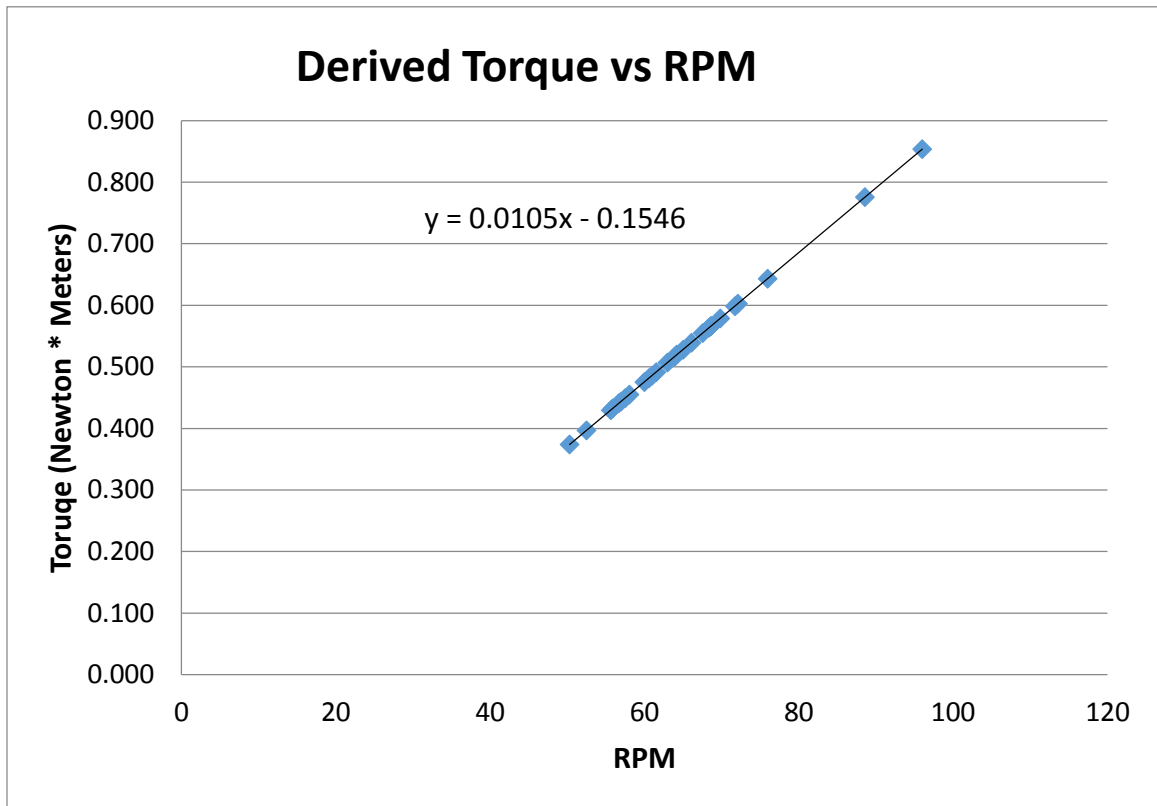


Figure 43: Derived Torque vs RPM

After observing the derived plot generated using the line of best fit, the team determined that the line is only applicable between the observed RPM range of 50 to 100 RPMs, as there was no collected data outside this range to support any further extrapolation.

## Chapter 8: Analysis

The wind speed, RPM, torque, and other results are analyzed further in the next chapter which led to some key findings. Due to the variance in the wind speed during the team's testing phases, the number of data points and relationships established in the results section, the analysis section uses the previously mentioned methods to further analyze the data.

### 8.1 Power

The first step in the analysis of the data was to calculate the power produced by the turbine. This was done using Equation 5 and the RPM, torque, and wind speed data.

To develop the relationship between power and wind speed, the team first used the nine wind speed data points observed during the RPM and wind speed testing. Using the data from the team's torque vs wind speed testing in chapter 7.3, the team was able to observe and record a value of torque for one of the nine wind speeds. If a wind speed from the RPM testing did not match a wind speed in torque testing then the line of best fit for Torque vs Wind Speed in chapter 7.3 was used to determine the torque value. The torque value was then used to find the power output of the turbine.

For some of the wind speeds observed the team was unable to find a torque based on the data collected alone. For these instances the team used Equation 18 to determine what the estimated torque would have been at that wind speed.

Once the team established nine torque values that correlated with a set of nine wind speeds, the team used the RPM data that corresponded with the nine wind speed points. In doing this, the team was able to produce Table 10 below.

Wind Speed (m/s)	RPM	Angular Velocity (rad/s)	Torque (N*m)	Power (W)
5.5	52.5	5.5	0.5	2.8
6.5	60.0	6.3	0.6	3.5
6.8	65.0	6.8	0.6	3.9
8.4	79.9	8.4	0.7	5.5
8.5	63.0	6.6	0.7	4.4
9	75.0	7.9	0.7	5.4
9.5	96.0	10.0	0.7	7.3
10.7	76.3	8.0	0.8	6.4
12	79.2	8.3	0.9	7.4

Table 10: Power to Wind Speed

From results compiled in Table 10 above the team plotted a graph of power to wind speed, shown below in Figure 44. The power produced by the turbine ranged from 2.8 W to 7.4 W.

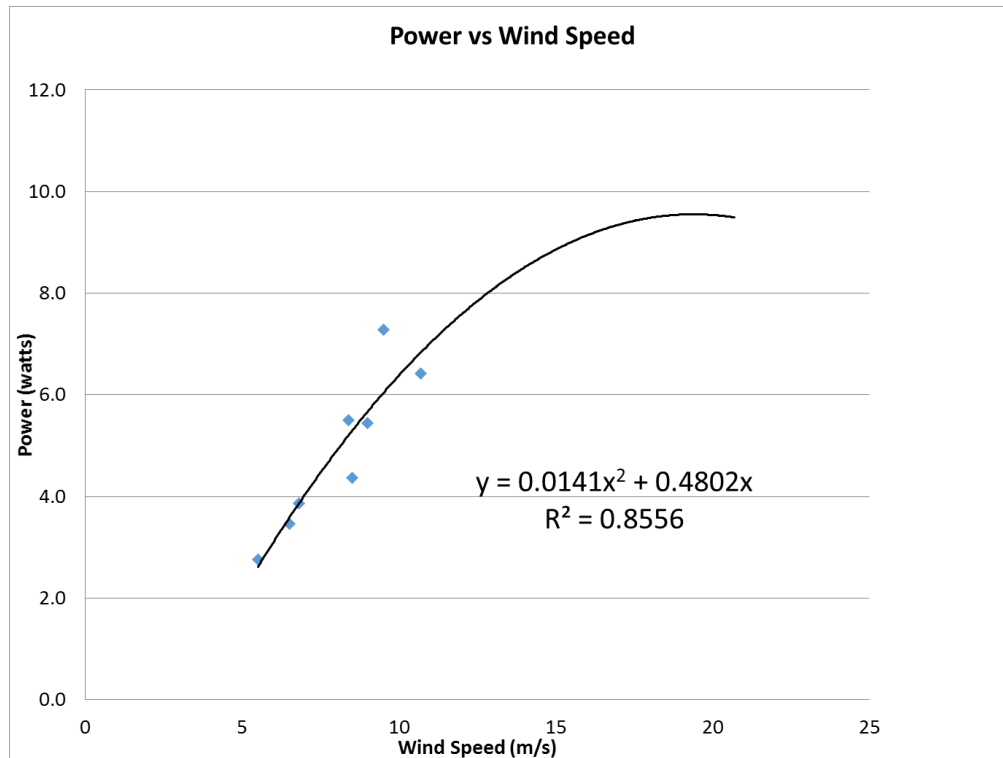


Figure 44: Calculated Power vs Wind Speed

The graph in Figure 44 above showed clear findings regarding the power data, including the relationship between the wind speed and how much power the turbine produced. The power generated by the turbine increased as the wind speed grew larger which was expected because the wind speed is the driving factor of the turbine power.

The line of best fit is plotted using a second order polynomial because that is the relationship observed in other VAWTs. This happens due to the fact that as the wind increases the power starts to reach a maximum before the turbine eventually produces less power. The graph above shows the extrapolation of a maximum wind speed reached and is accurate based on the data indicated by the  $R^2$  correlation of 0.86. If the team had been able to test at wind speeds of up to 15 m/s the data suggests that the turbine could have produced a power output as high as 9 W.

## 8.2 Efficiency

Once the power and torque of the turbine were plotted, the team moved on to find the efficiency of the turbine. The efficiency is a relationship of the power coefficient and tip speed ratio of the turbine. The power coefficient is a dimensionless parameter used to

easily compare different types of turbines. It is a ratio of the power produced by the turbine over the total power available from the wind as defined by Equation 20 below.

$$\text{Power coefficient} = \frac{\text{Power}}{.5 * \rho * A * U^3}$$

Equation 20: Power Coefficient

The tip speed ratio is another dimensionless parameter which relates the speed of the turbine rotation and the speed available in the wind. It is a relationship between the velocity of the wind and the angular velocity and radius of the turbine. The tip speed ratio was calculated using Equation 7 in chapter 4.

The graph shown in Figure 45 below shows the efficiencies of the turbine as a relationship between the power calculated in Chapter 8.1 and the calculated tip speed ratio. The line of best fit is a second order polynomial because the relationship between the power coefficient and tip speed ratio simplifies to  $U^2$ . On a fully realized graph for a turbine, the data tends to be a downward facing parabola; the team's data currently covers the lowest end of the parabola.

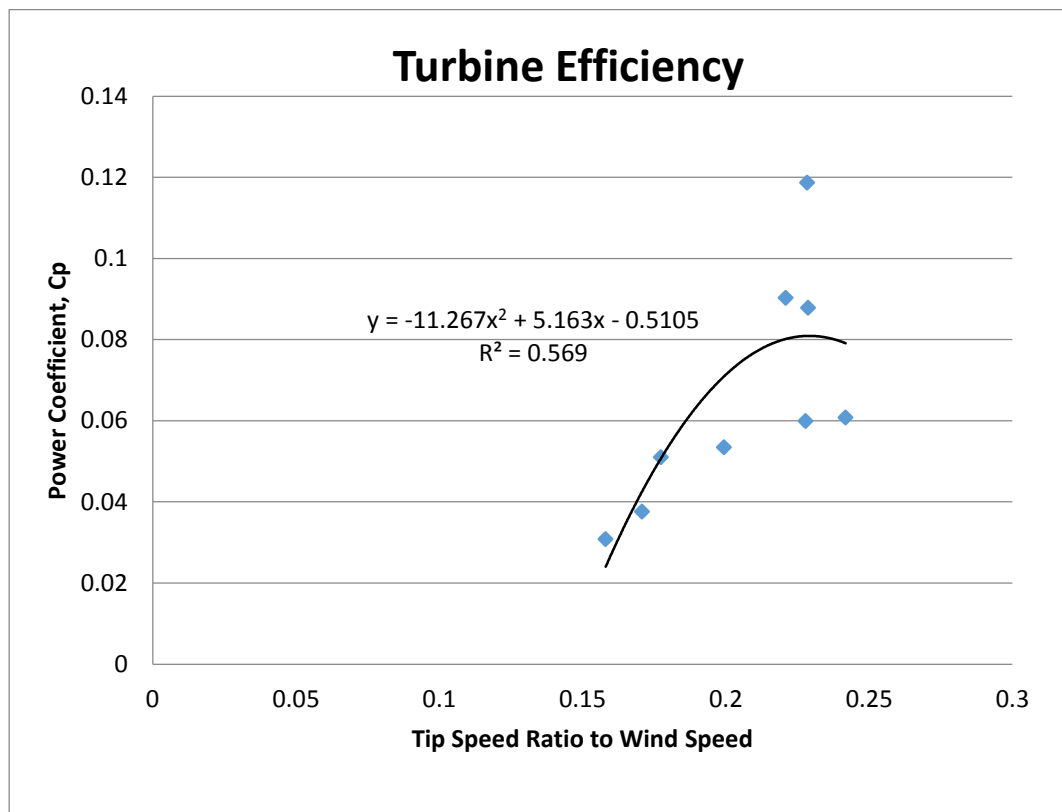


Figure 45: Turbine Efficiency

The graph shows efficiencies ranging from 3 to 12% and tip speed ratios from 0.15 to 0.25. The data was concentrated for values with a tip speed ratio between 0.15 and 0.20 with efficiencies ranging from 3 to 6%. These values are concentrated because there is

not a large difference in power produced at these points. When the tip speed ratio became greater than 0.20 the efficiencies were more unpredictable as they had a larger range, from 6 to 12%. This large discrepancy was due to the difference in available power as the wind speeds vary between 5.5 and 9.5 m/s for tip speeds ratio greater than 0.20. This difference of 4 m/s was exposed when the wind speed is cubed in the power available equation demonstrated in Equation 20. This result means that as the wind speed increases, the efficiency of the turbine decreases.

The maximum efficiency produced was calculated to be 12%; however the line of best fit indicates a value of 8 to 10%. The variance in efficiencies as the tip speed ratio increased led to a  $R^2$  value of 0.57, as seen in the figure above, which led to unpredictability especially as the tip speed ratio increased. The line was plotted based on the local sample size; however it does indicate that the efficiency is starting to level off at a value of 8% and that this is the maximum efficiency of the turbine. If the team had been able to obtain more results particularly those at higher tip speed ratios, the efficiency may have continued to increase.

## Chapter 9: Conclusions

After collecting, plotting, and analyzing the team's testing results, the team was able to draw several conclusions of the first generation prototype turbine. The first conclusion from testing was that the articulating airfoil design was able to start at a lower wind velocity than the fixed design. Due to the fact that the fixed design turbine did not start rotating, no conclusions can be drawn between the two designs in terms of which one rotated faster, produced more power, or was more efficient. The data collected for the articulating design was analyzed to conclude the speed, power, and efficiency of the turbine.

The articulating design started rotating at a speed of 6 m/s and rotated at speeds of 50 to 100 RPMs at wind speeds of 5 m/s to 12 m/s. The team was able to observe RPM data as low as 5 m/s because the turbine only needed 6 m/s to start but could operate at lower wind speeds. The turbine was able to start rotating after overcoming the static friction which was calculated at a force of 1.12 N which is a torque of 0.25 N\*m. The 0.25 N\*m was calculated by multiplying the force by the moment arm which in this case was the radius of the turbine, 0.22 m. This led to a torque generated between 0.3 and 0.9 N\*m with a power production between 2.8 and 7.4 W while the team expected a range of 5.4 to 24.6 W, as demonstrated in Chapter 4. The relationship between this power production and the speeds of the turbine led to efficiencies fluctuating between 3 to 12%. The 12% efficiency was the maximum efficiency observed; however this is believed to be an outlier and therefore the actual ideal efficiency was concluded to lie between 8% and 10%. The driving factor that affect the power and efficiency of the turbine was the wind speed as described in the analysis section.

## Chapter 10: Recommendations

During design, manufacturing and testing of the wind turbine, the team encountered several areas which could be improved in order to increase the efficiency of the turbine. Below are some of the recommendations the team has for any potential future work on a similar turbine.

### 10.1 Friction

One of the problems which was anticipated in the design portion of the project was the friction that would be encountered. The starting wind velocity for the turbine was found to be approximately 6 m/s and the starting velocity could have been decreased by lowering the areas of friction in the turbine. One area of high friction was the ball bearings supporting the base plate on the table. Another area of high friction is the right angle connection piece.

For future experiments, there would be several possibilities for decreased friction in the system. The first possibility would be to source or manufacture high precision bearings in all current instances in the system and ensure that all bearing are properly greased and maintained. The second possibility would be to exchange the current bolt and spacer system for mounting the airfoils with a high precision bearing system that would be installed at the attachment point to the turbine plate. The third possibility for reducing friction would be to develop a system that would eliminate the right angle adjustment piece by recording all data from the vertical axis.

### 10.2 Manufacturing

In order to further improve the performance of the turbine, the manufacturing of the airfoils could also have been improved. With better experience in manufacturing and access to an industrial large scale foam cutter, the airfoils could have been made more uniform. The process of stacking the 2 inch foam pieces and gluing them together introduced several inconsistencies in the airfoils which made the three not similar to each other. If the airfoils had been made more similar in geometry, the performance could again improve.

Another aspect of the airfoils that could have been improved upon was the material which they were made out of. One manufacturing consideration would be to construct the airfoils from a material that would be lightweight and have a smoother surface finish. Examples of potential materials to be looked into would be a 3D plastic airfoil or a rolled aluminum frame.

Another limitation that the team found during the manufacturing process was the laser cutter which the team had access to. The laser cutter on campus has a maximum geometry of 18 inches. This meant that the acrylic plates could not be manufactured to a size larger than 18 inches in diameter. As was discussed in the design section above, a

larger diameter turbine would yield a higher power output. Therefore the team had originally looked into other methods of producing a larger diameter base plate, but it was determined that more problems would be encountered which would ultimately reduce the performance of the turbine. Some of the foreseen problems included manufacturing time and the ability to make a perfect circle while keeping the weight as low as possible.

### 10.3 Testing

During testing it was also found that the results gathered for both the fixed and the articulating airfoils were limited to the inconsistent and somewhat low wind velocities. Testing was done on campus and at the Worcester Regional Airport. These were the two accessible locations where the highest wind velocities were found. However, at these wind velocities, the team was still unable to reach a high enough wind velocity for the fixed airfoils to start spinning. Based on the calculations explained in previous sections, the team estimated that there was potential for the fixed airfoils to output power, but this was not observed at the wind velocities that were achieved during testing. During the on campus testing it was also found that the wind came in bursts as opposed to a constant airflow. With more consistent airflow, more consistent data could have been collected.

The team considered many possible alterations for the testing procedure, which could be implemented in future experiments. One major alteration for the testing procedure would be to develop a testing method that would record all three major data points concurrently. A process that could achieve this would be through data acquisition software with electronic input from sensors. This would further assist in the startup torque calculations and turbine efficiency calculations.

## References

- F.L. Pontaa, J. S. (2005). The aerodynamics of variable-geometry oval-trajectory Darrieus Wind Turbines. *Elsevier*.
- International Energy Agency. (2015). *Renewables*. Retrieved from Wind: <http://www.iea.org/newsroomandevents/news/2013/october/wind-power-seen-generating-up-to-18-of-global-power-by-2050.html>
- Ironman Windmill. (2011). *Water Pumping windmill History in America*. Retrieved from Water Pumping windmill: <http://www.ironmanwindmill.com/windmill-history.htm>
- John D. Anderson, J. (2010). *Fundamentals of Aerodynamics*. New York: McGraw Companies - Hill.
- Jurgens, D., Palm, M., Singer, S., & Urban, K. (2005). *Numerical Optimization of the Voith-Schneider Propellor*. Universitat Ulm.
- Kaprawi Sahim, K. I. (2014). Experimental Study of Darrieus-Savonius Water Turbine with Deflector: Effect of Deflector on the Performance. *International Journal of Rotating Machinery*.
- Letcher, T. (n.d.). *Small Scale Wind Turbines Optimized for Low Wind Speeds*. Columbus, OH: The Ohio State University.
- Muhammad Mahmood Aslam Bhutta, N. H. (2011). Renewable and Sustainable Energy Reviews. *Elsevier*, 6-13.

Muhammad Mahmood Aslam Bhutta, N. H. (2011). Renewable and Sustainable Energy Reviews. *Elsevier*, 6-13.

NASA. (2015). *Global Climate Change*. Retrieved from The current and future consequences of global change: <http://climate.nasa.gov/effects/>

REUK. (2014). *Darrieus Wind Turbines*. Retrieved from REUK - The Renewable Energy Website: <http://www.reuk.co.uk/Darrieus-Wind-Turbines.htm>

Sandra Eriksson, H. B. (2008). Evaluation of different turbine concepts for wind power. *Elsevier*, 2-14.

Shuttleworth, M. (2014). *Heron's Invention*. Retrieved from Explorable: <https://explorable.com/heron-inventions>

United States Environmental Protection Agency . (2015). *Overview of Greenhouse gases*. Retrieved from Climate Change: <http://www.epa.gov/climatechange/ghgemissions/gases/co2.html>

Yamada, H. (n.d.). Voith-Schneider Propeller. *Fuji*, 115-126.

## Appendix A: Predicted Lift and Drag Algebra

Once the lift and drag forces are found, the resultant force must be identified. The resultant force is based on the relationship between the lift and the drag. This is shown below in Equation 21.

$$\vec{R} = (D_x + L_x) \hat{i} + (D_y + L_y) \hat{j}$$

*Equation 21: Resultant equation*

Where the sum of the x components of the lift and drag equals the x component of the resultant force.

The x and y components of the forces can be found using Equation 22, Equation 23, Equation 24, Equation 25 below. These equations assume a positive angle of attack.

$$L_x = L \sin(\alpha)$$

*Equation 22: Lift force in X-Direction-Positive angle of attack*

$$L_y = L \cos(\alpha)$$

*Equation 23: Lift Force in Y-Direction-Positive angle of attack*

$$D_x = D \cos(\alpha)$$

*Equation 24: Drag Force in X-Direction-Positive angle of attack*

$$D_y = D \sin(\alpha)$$

*Equation 25: Drag Force in Y-Direction-Positive angle of attack*

Using those components you can calculate the resultant force in Equation 26.

$$\vec{R} = (D \cos(\alpha) - L \sin(\alpha)) \hat{i} + (D \sin(\alpha) + L \cos(\alpha)) \hat{j}$$

*Equation 26: Resultant Force-Positive angle of attack*

If the angle of attack is negative, it requires a slightly different set of equations (Equation 27, Equation 28, Equation 29, Equation 30, Equation 31, Equation 32)

$$L_x = L \sin(\alpha)$$

*Equation 27: Lift Force X-Direction-Negative angle of attack*

$$L_y = L \cos(\alpha)$$

*Equation 28: Lift Force Y-Direction-Negative angle of attack*

$$D_x = D \cos(\alpha)$$

*Equation 29: Drag Force X-Direction-Negative angle of attack*

$$D_y = -D \sin(\alpha)$$

*Equation 30: Drag Force Y-Direction-Negative angle of attack*

$$\vec{R} = (D_x + L_x) \hat{i} + (D_y + L_y) \hat{j}$$

*Equation 31: Resultant Force Equation 1-Negative angle of attack*

$$\vec{R} = (D \cos(\alpha) + L \sin(\alpha)) \hat{i} + (L \cos(\alpha) - D \sin(\alpha)) \hat{j}$$

*Equation 32: Resultant Force Equation 2-Negative angle of attack*

## Appendix B: Detailed Predictive Calculations

Blade Number	1.00	2.00	3.00	4.00	5.00	6.00
Theta (Degrees)	0.00	60.00	120.00	180.00	240.00	300.00
Theta (radians)	0.00	1.05	2.09	3.14	4.19	5.24
Alpha (radians)	0.00	0.55	1.14	0.00	-1.14	-0.55
Alpha (degrees)	0.00	31.74	65.21	0.00	-65.21	-31.74
W (true speed) (m/s)	9.50	8.23	4.77	0.50	4.77	8.23
Coefficient of Lift	0.25	1.50	1.83	0.25	-1.34	-1.01
Lift (N)	1.52	6.80	2.79	0.00	-2.04	-4.58
Coefficient of Drag	0.02	0.04	0.05	0.02	0.06	0.04
Drag (N)	0.11	0.17	0.08	0.00	0.09	0.18
Resultant Force (N)	0.11	-3.43	-2.50	0.00	1.89	2.56
Torque (N*m)	0.02	-0.78	-0.57	0.00	0.43	0.59
Power (W)	0.49	-15.44	-11.24	0.00	8.51	11.54
Power Position 1 (W)	-2.24			Average Power (W):		-3.07
Power Position 2 (W)	-3.90					

## Appendix C: Computer Aided Design Drawings

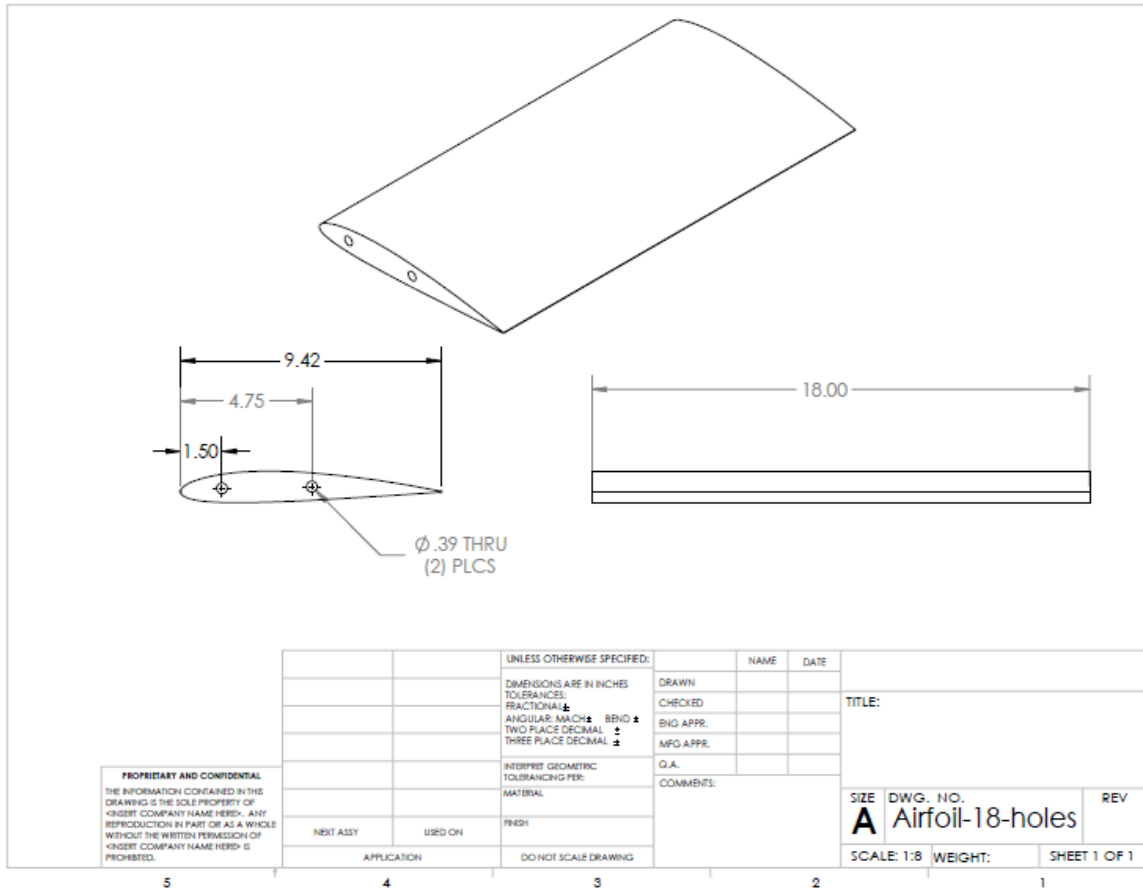


Figure 46: Airfoil Design

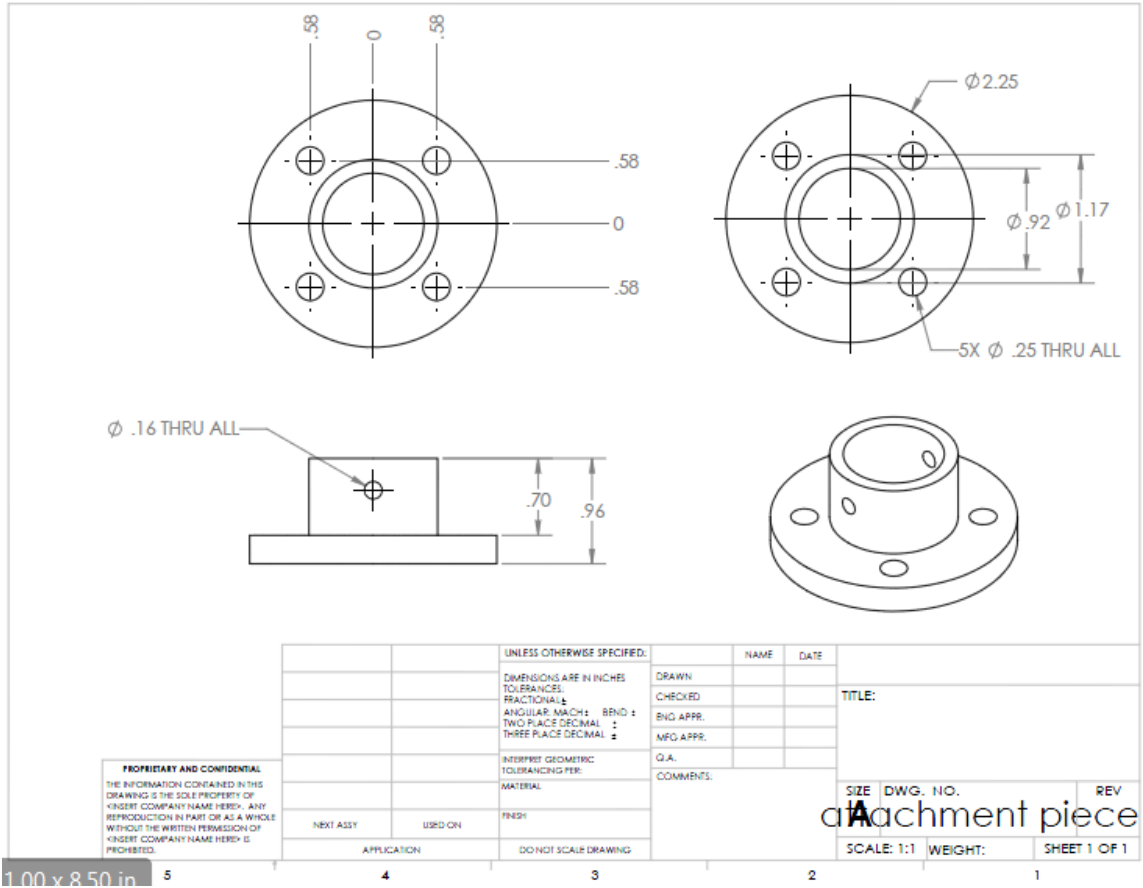


Figure 47: Attachment Piece Design

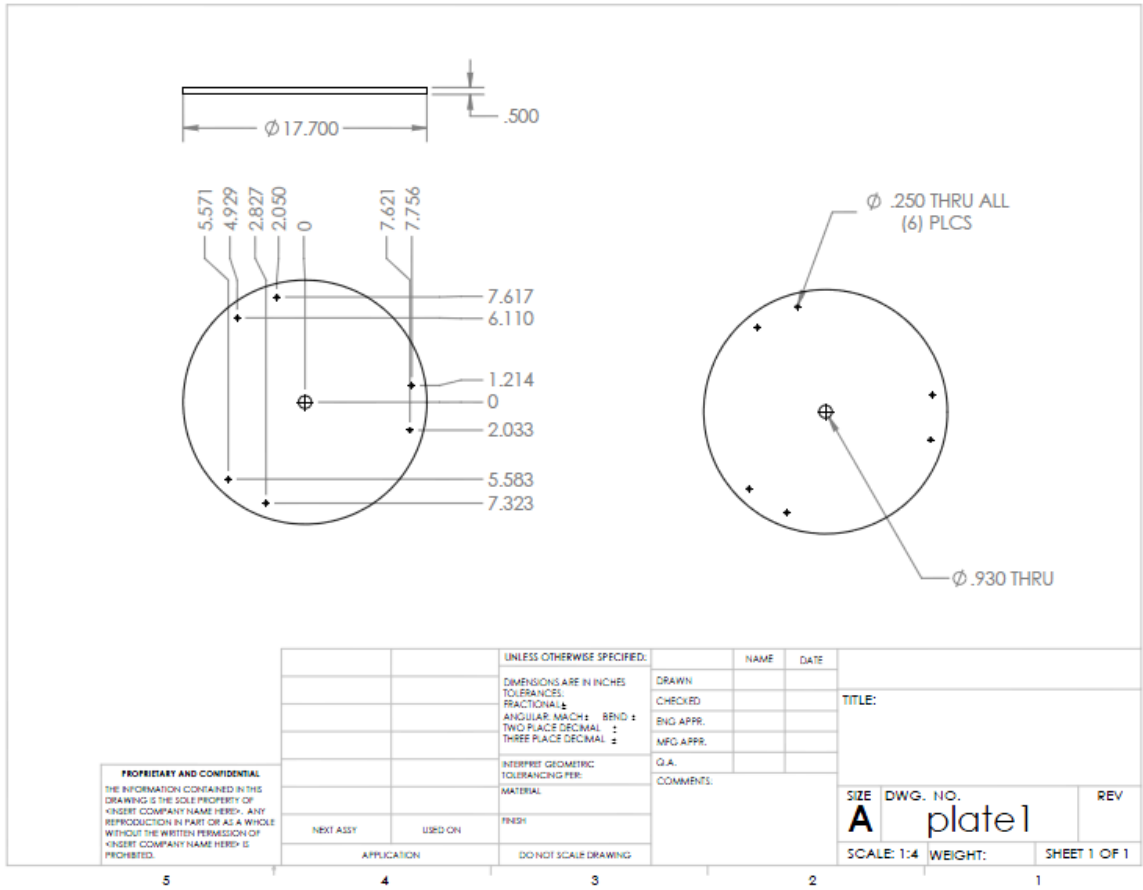


Figure 48: Acrylic Base Plate Design

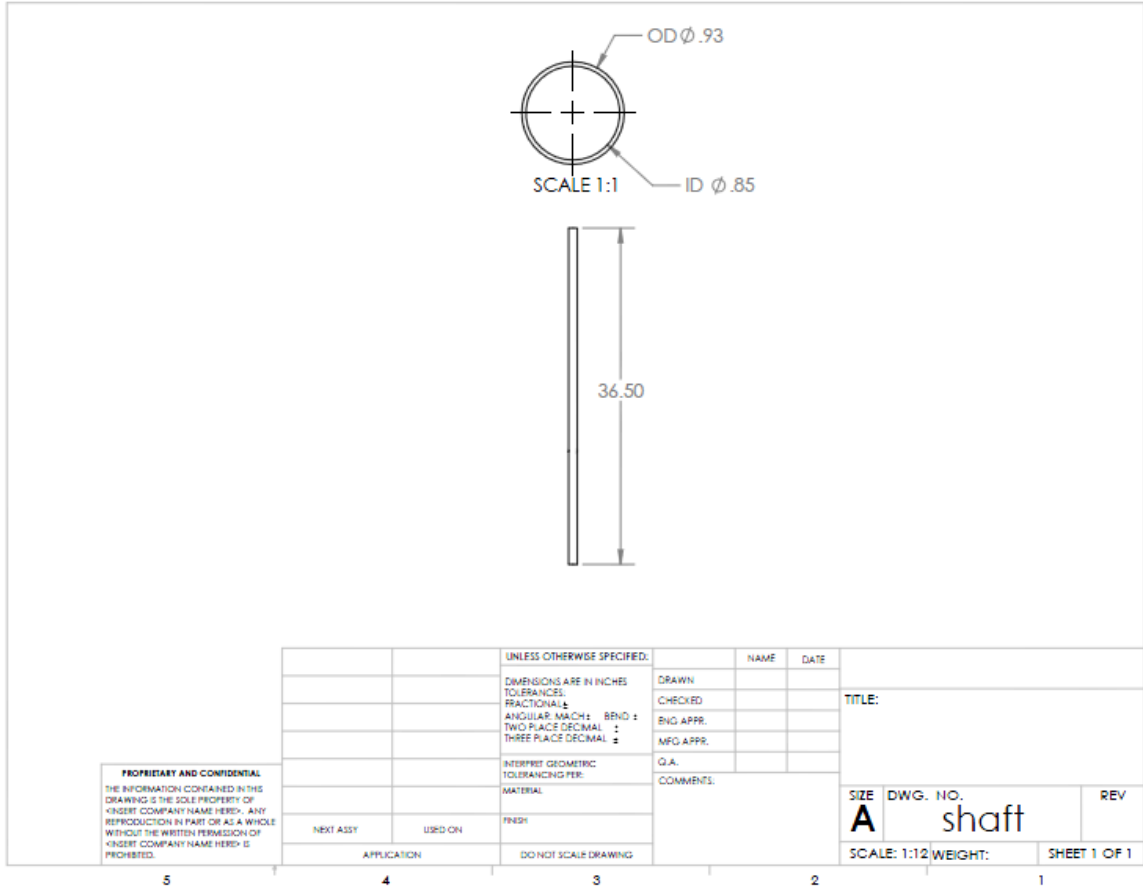


Figure 49: Shaft Design

## Appendix D: Turbine Starting Time Calculations

Below are the equations used in order to find the starting time of the turbine.

$$\sum \text{Torques} = \text{Torque}_{\text{starting}} - \text{Torque}_{\text{static friction}}$$

*Equation 33: Sum of Torques in operation*

$$\sum \text{Torque} = 0.53 \text{ Nm} - 0.25 \text{ Nm} = 0.23 \text{ Nm}$$

*Equation 34: Evaluated sum of torques*

$$a = \frac{\sum \text{Torques}}{\text{Moment of Inertia}}$$

*Equation 35: Angular acceleration*

$$a = \frac{0.28 \text{ Nm}}{0.40 \text{ Kgm}^2} = 0.7 \frac{\text{rad}}{\text{s}^2}$$

*Equation 36: Evaluated angular acceleration*

$$\omega = a * t$$

*Equation 37: Angular velocity with regards to time*

$$\int \omega = \int a * t$$

*Equation 38: Angular velocity integral*

$$\theta = \frac{1}{2} at^2$$

*Equation 39: Angular position with regards to time*

$$2.09 \text{ rad} = \frac{1}{2} * 0.7 \frac{\text{rad}}{\text{s}^2} * t^2$$

*Equation 40: Evaluated angular position with regards to time*

$$t = 2.44 \text{ s}$$

Using a model developed in SolidWorks, the team found that the moment of inertia of the system was 1381 lb\*in<sup>2</sup> (0.40 kg\*m<sup>2</sup>). This is shown in Figure 50 below.

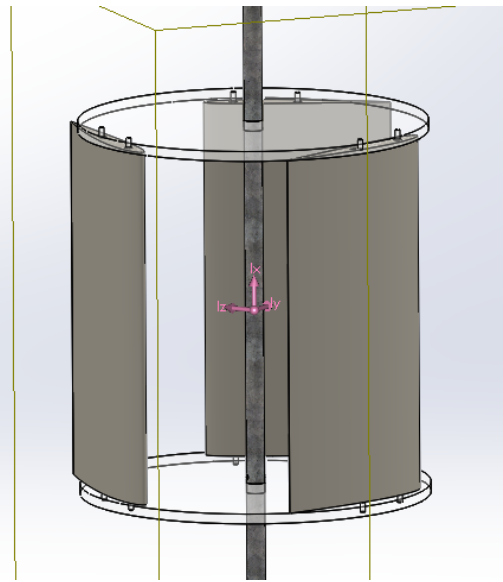
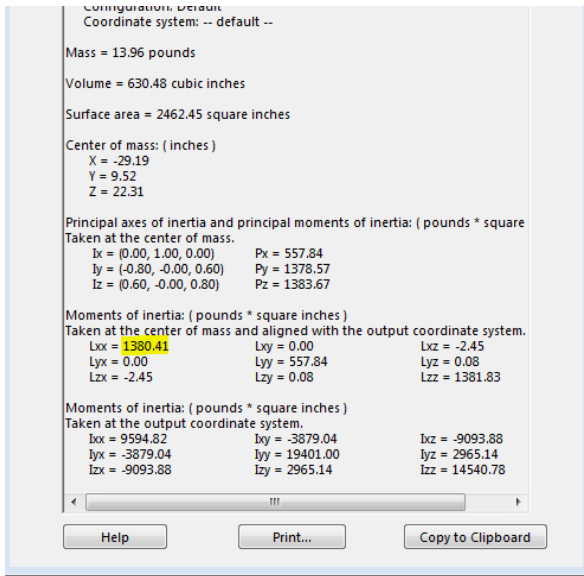


Figure 50: SolidWorks Inertia

## Appendix E: Torque Testing Results

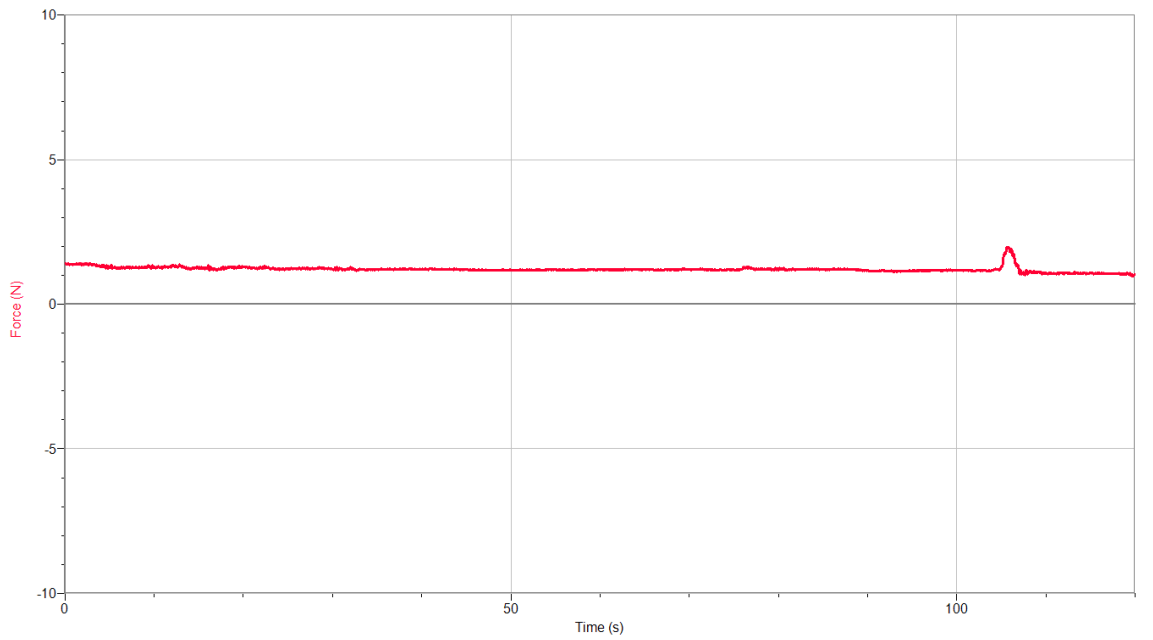


Figure 51: Torque Testing Graph 1

Seconds	Wind Speed (m/s)	Force (N)
20	5.8	0.796
40	6	0.921
60	7	1.652
80	7	0.939
100	6.4	1.107
105	9.2	1.826
120	6.2	1.101

Table 11: Torque Testing Analysis 1

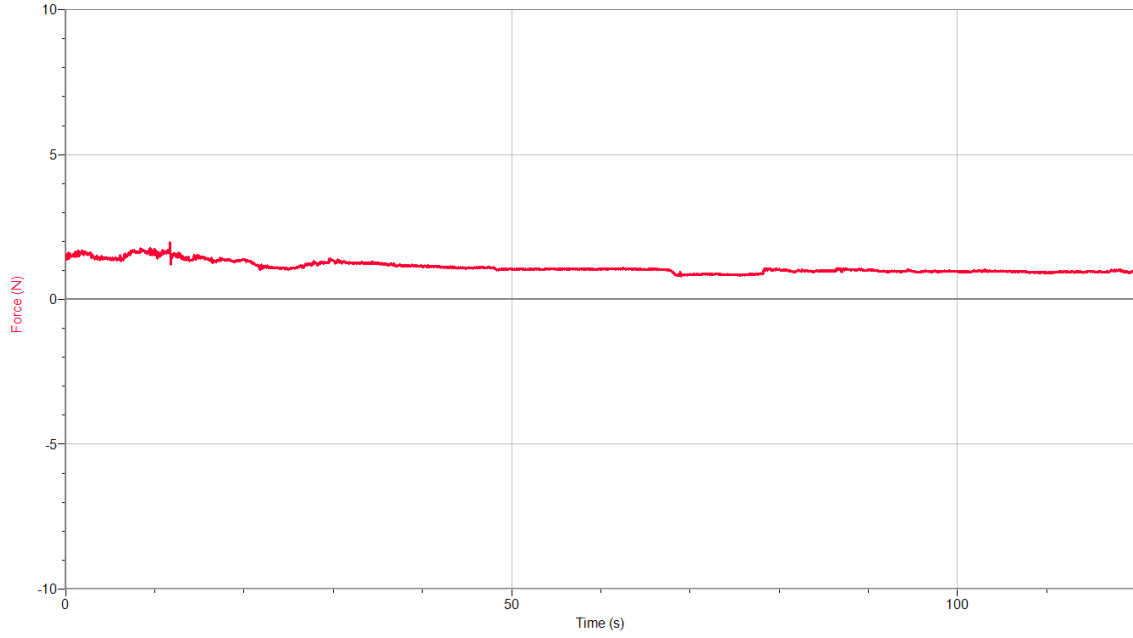


Figure 52: Torque Testing Graph 2

Seconds	Wind Speed (m/s)	Force (N)
20	8	1.37
40	5.8	1.149
60	5	1.047
80	4	1.035
100	5	0.957
120	6.6	0.945

Table 12: Torque Testing Analysis 2

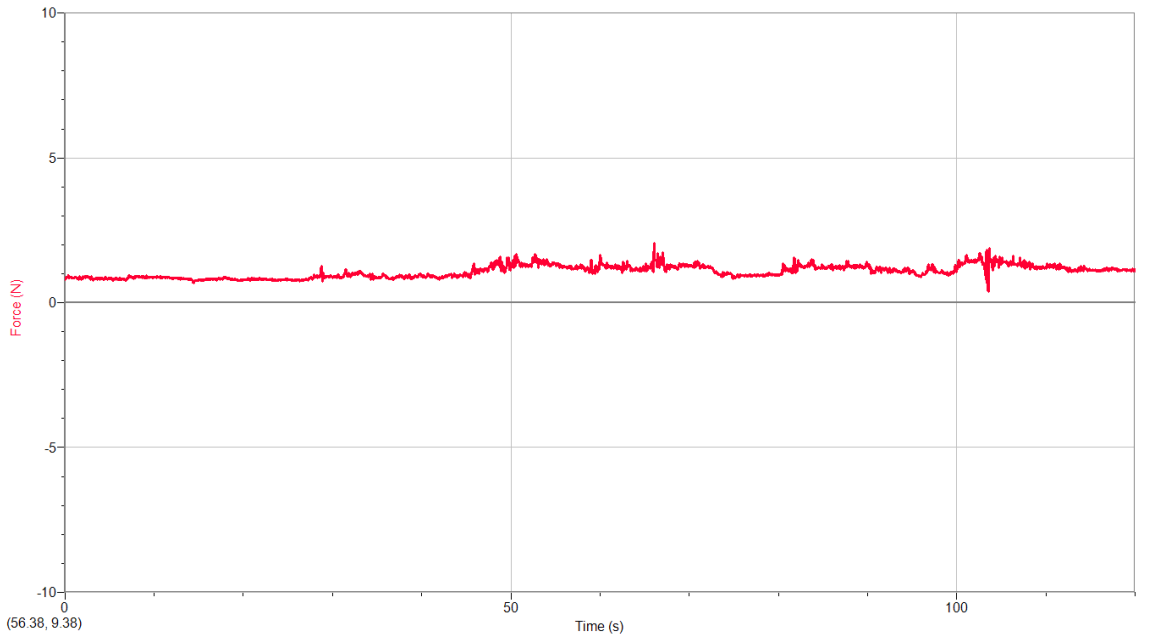


Figure 53: Torque Testing Graph 3

Seconds	Wind Speed (m/s)	Force (N)
20	6	1.284
40	4.9	1.206
60	3.8	1.2
80	4.6	1.206
100	4.9	1.182
120	5	1.026

Table 13: Torque Testing Analysis 3

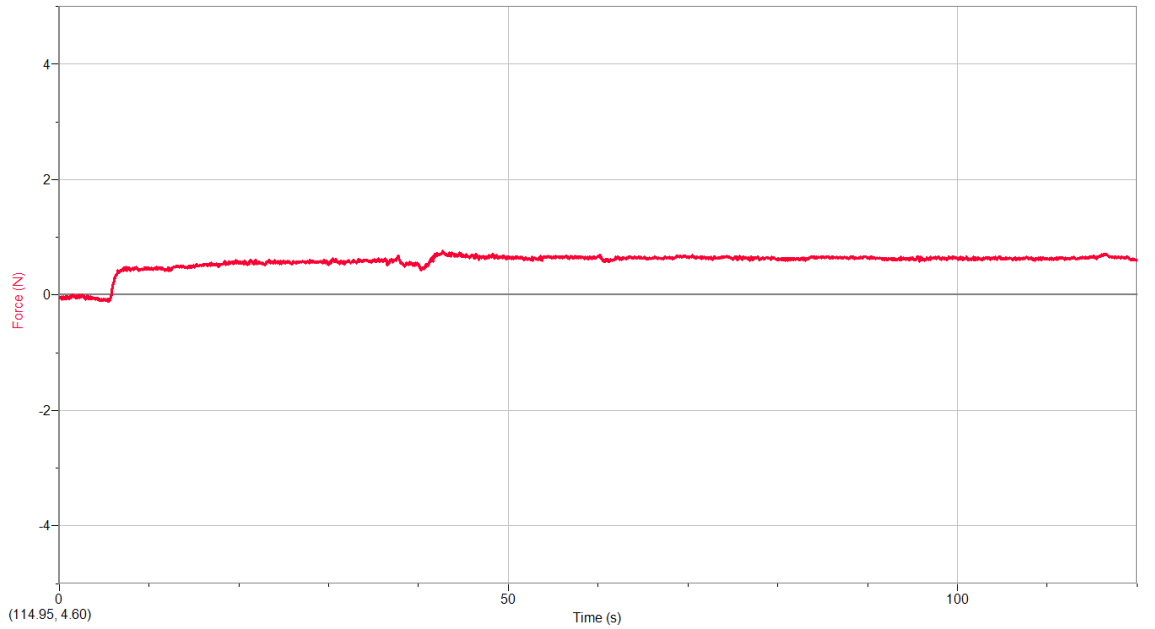


Figure 54: Torque Testing Graph 4

Seconds	Wind Speed (m/s)	Force (N)
20	6	0.552
40	6.8	0.541
60	7	0.66
80	6.5	0.63
100	6	0.636
120	7	0.606

Table 14: Torque Testing Analysis 4